

# Numerical solution of steady-state groundwater flow and solute transport problems: Discontinuous Galerkin based methods compared to the Streamline Diffusion approach

A.Q.T. Ngo<sup>1</sup>, P. Bastian<sup>1</sup>, O. Ippisch<sup>1,2</sup>

<sup>1</sup>University of Heidelberg, Interdisciplinary Center for Scientific Computing, Im Neuenheimer Feld 368, 69120 Heidelberg, Germany

<sup>4</sup>Clausthal University of Technology, Department of Mathematics, Erzstraße 1, 38678 Clausthal-Zellerfeld, Germany

Email: adrian.ngo@iwr.uni-heidelberg.de

## Abstract

In this study, we consider the simulation of sub-surface flow and solute transport processes in the stationary limit. In the convection-dominant case, the numerical solution of the transport problem may exhibit non-physical diffusion and under- and overshoots. For an interior penalty discontinuous Galerkin (DG) discretization, we present a  $h$ -adaptive refinement strategy and, alternatively, a new efficient approach for reducing numerical under- and overshoots using a diffusive  $L^2$ -projection. Furthermore, we illustrate an efficient way of solving the linear system arising from the DG discretization. In 2-D and 3-D examples, we compare the DG-based methods to the streamline diffusion approach with respect to computing time and their ability to resolve steep fronts.

## 1 Introduction

Natural flowing conditions that are nearly at steady-state over a long period of time (i.e. several days during which a tracer experiment is being conducted) can be expected, if at all possible, in a confined aquifer. Due to very small dispersivities and very small molecular diffusion, (non-reactive) solute transport in groundwater is convection-dominated. Considering temporal moments of its concentration leads to the *steady-state singularly perturbed convection-diffusion equation*. The numerical solution of this kind of equations has a long tradition. Due to the fact that a linear monotonicity preserving scheme can be at most first-order accurate (Godunov's Theorem), all existing schemes suffer from a trade-off between numerical diffusion (too much smearing) and spurious oscillations (under- and overshoots) near internal or bound-

ary layers where the gradient of the solution is very large (steep fronts). From a practical point of view, the decision whether the one or the other deficit is tolerated has to be made, leading to the appropriate choice of a numerical scheme.

Amongst the vast literature on the subject, the books of [Roos et al. \[2008\]](#) and [\[Kuzmin, 2010\]](#) provide excellent overviews of state-of-the-art classes of schemes. We give a short overview of the most prominent methods, list their main advantages and disadvantages, hereby drawing on the results presented by [Augustin et al. \[2011\]](#), who have worked on a special 2-D problem (Hemker problem). They compared the numerical solutions at specific cut lines with respect to the size of maximal under- and overshoots, the width of smeared internal layers and the performance in computing time, revealing important properties of the different schemes.

- The Scharfetter-Gummel scheme is a first-order finite volume scheme. It is efficient and oscillation-free, but the solution is strongly smeared at layers. A higher order extension is not available.
- The Streamline Diffusion finite element method (SDFEM), also known as Streamline Upwind Petrov-Galerkin (SUPG) method, adds a residual-based stabilization term to the standard Galerkin method [\[Brooks and Hughes, 1982\]](#). SDFEM belongs to the less time-consuming methods that are capable of resolving the steep fronts well. Due to its simplicity, it has been the mainstream approach for decades and a standard method in the hydrogeologists' community [\[Cirpka and Kitanidis, 2001; Nowak and Cirpka, 2006; Gordon et al., 2000; Couto and Malta, 2008; Bear and Cheng, 2010\]](#) where our practical application originates from. However, the optimal choice of a user-defined stabilization parameter is an open question.
- The Continuous Interior Penalty (CIP) method [\[Roos et al., 2008\]](#) adds a symmetric stabilization term to the standard

Galerkin method that penalizes jumps of the gradient across faces (edge stabilization technique). It introduces connections between unknowns of neighboring mesh cells and leads to a discretization with a wider matrix stencil. Compared to the SDFEM method it is in general less performant.

- Spurious Oscillations at Layers Diminishing (SOLD) methods, originally developed in [\[Hughes et al., 1986\]](#) and further investigated in [\[John and Knobloch, 2007a,b, 2008\]](#), suppress oscillations caused by SDFEM by adding a further stabilization term introducing diffusion orthogonal to streamlines (crosswind diffusion). This term is in general non-linear. Therefore, a non-linear equation has to be solved for a linear problem. Furthermore, the stabilization term contains another user-defined parameter whose optimal choice might become difficult for complicated problems. SOLD methods are capable of reducing numerical oscillations at a higher computational cost. The larger the stabilization parameter, the better the reduction. However, non-linearity also increases and the iterative non-linear solver might not converge [\[Augustin et al., 2011\]](#).
- Algebraic Flux Correction (AFC) is a general approach to design high resolution schemes for the solution of time-dependent transport problems that ensure the validity of the discrete maximum principle [\[Kuzmin, 2006, 2010\]](#). Whereas the aforementioned stabilization methods modify the bilinear form of a finite element method (FEM), AFC methods modify the linear system arising from a FEM discretization by adding discrete diffusion to the system matrix and appropriate anti-diffusive fluxes to the right hand side. The anti-diffusive fluxes are non-linearly dependent on the computed solution. Depending on whether the algebraic constraints are being imposed on the semi-discrete or the fully discrete level,

flux limiters of TVD-type (total variation diminishing) or FCT-type (flux corrected transport) can be constructed. Only the FEM-TVD schemes can be used to solve the steady-state convection-diffusion equation directly. Using FEM-FCT schemes, a pseudo time stepping to the stationary limit of the associated time-dependent problem would deliver the steady-state solution [Kuzmin, 2006]. A suitable linearization technique for the anti-diffusive fluxes exists only for the FEM-FCT scheme [Kuzmin, 2009]. According to the studies in [John and Schmeyer, 2008, 2009], FEM-FCT schemes yield qualitatively the best solution and, beyond that, the linear FEM-FCT scheme is efficient. The authors recommend the linear FEM-FCT for the solution of instationary problems. Linearized AFC-based methods for the solution of the stationary transport problem are not available.

- Discontinuous Galerkin (DG) methods use piecewise polynomials, that are not required to be continuous across faces, to approximate the solution. The total number of degrees of freedom on a structured mesh with cuboidal cells is  $O(n \cdot (k+1)^d)$  where  $n$  is the number of mesh cells,  $d$  is the dimension of the domain and  $k$  is the polynomial degree. Compared to a continuous Galerkin FEM method, a DG method using the same polynomial space on the same structured mesh requires more unknowns. This disadvantage is balanced by a long list of advantages that has made DG increasingly attractive in computational fluid dynamics in the last decade: DG methods are readily parallelizable, lead to discretizations with compact stencils (i.e. the unknowns in one mesh cell are only connected to the unknowns in the immediate neighboring cells), a higher flexibility in mesh design (non-conforming meshes are possible in adaptive h-refinement) and the availability of different polynomial degrees on different mesh cells (adaptive p-refinement). Furthermore, DG schemes sat-

isfy the local, cell-wise mass balance which is a crucial property for transport processes in a porous medium. They are particularly well-suited for problems with discontinuous coefficients and effectively capture discontinuities in the solution. In the comparative study by [Augustin et al., 2011], the DG method gives the best results regarding sharpness of the steep fronts and produces small errors with respect to reference cut lines, whereas under- and overshoots are larger than those produced by the SDFEM method. For the discretization of first-order hyperbolic problems, upwinding is incorporated into the formulation of DG schemes, evading the need for user-chosen artificial diffusion parameters. The books of Kanschat [2008a], Rivière [2008] and Pietro and Ern [2012] offer a comprehensive introduction to this class of methods.

For time-dependent problems, where explicit time stepping schemes combined with finite volume or DG discretizations can be used, slope limiters may be constructed from the solution of one time-step to preserve monotonicity in the following time-step. To the best of our knowledge, for the immediate solution of stationary problems, a post-processing technique of this type is not available.

In the simulation of many applications (e.g. biochemical reactions or combustion), the concentration of a species must attain physical values (numerical under- and overshoots are not accepted) although the position of the plume may be allowed to be inaccurate. Our practical application stems from the field of geostatistical inversion [Cirpka and Kitanidis, 2001] in which the hydraulic conductivity is estimated on the basis of indirect measurements of related quantities such as the tracer concentration or arrival time. The computed solution of the transport problem is used for a pointwise comparison with real measurements. Hereby, the parameter estimation scheme allows for measurement errors, i.e. a small amount ( $\approx 5\%$ ) of spurious oscillations in the solution is tolerable. By contrast, the

correct localization of steep fronts is of primary interest.

For high resolution 3-D simulations of real-world applications, direct sparse solvers are limited by their memory consumption. The main purpose of the stabilization term in the SDFEM method is not only to provide a solution with bounded under- and overshoots but also to improve the iterative solvability of the linear system arising from the SDFEM discretization. For an upwind scheme applied to a first-order hyperbolic problem, it is well-known that numbering the unknowns in a fashion that follows approximately the direction in which information is propagated will improve the performance and stability of iterative linear solvers of ILU or Gauss-Seidel type [Bey and Wittum, 1997; Hackbusch and Probst, 1997; Reed and Hill, 1973].

Motivated by the requirements for our practical application, we have chosen a DG-based method to solve the solute transport problem. The remaining part of this paper is structured as follows: Section 2 introduces the steady-state groundwater flow and solute transport equations, in Section 3 we consider two combinations of discretizations for their numerical solution: FEM/SDFEM and CCFV/DG.

- We present two approaches to reduce the under- and overshoots of the DG-solution of the transport problem:
  1. The first approach (Section 4) uses  $h$ -adaptive hanging-nodes 1-irregular refinement on a cuboidal axis-parallel mesh based on the residual error estimator by Schötzau and Zhu [2009] combined with an error-fraction marking strategy.
  2. The second approach (Section 5) is a diffusive  $L^2$ -projection of the DG solution into the continuous Galerkin finite element subspace. It works directly on the structured coarse mesh.
- In addition, we have implemented an efficient way to solve the linear system for the

DG discretization iteratively by exploiting a downwind cell-wise numbering of unknowns *before* the stiffness matrix is assembled (Section 6).

Numerical studies are presented in Section 7. The DG method is compared to a first order SDFEM implementation within the same code, i.e. the performance of the two different discretizations can be compared on the same computational grid using the same linear solver. The results are summarized in Conclusion & Outlook section.

The numerical software used to perform the simulations is written in C++ and based on the libraries of the *Distributed and Unified Numerics Environment* DUNE [Bastian et al., 2008b,a, 2011] and the finite element discretization module DUNE-PDELab ([www.dune-project.org/pdelab](http://www.dune-project.org/pdelab)). DUNE offers a structured parallel grid (YASP) and interfaces to the unstructured grids UG [Bastian et al., 1997] and DUNE-ALUGrid [Dedner et al., 2014].

## 2 Model equations

The physical models describing flow and transport processes in a confined aquifer are well developed and can be found in the textbooks [Bear and Cheng, 2010; De Marsily, 1986] or in the lecture note [Roth, 2012].

### 2.1 Groundwater flow

For convenience, we assume  $\Omega \subset \mathbb{R}^d$ ,  $d \in \{2, 3\}$  to be a rectangular cuboid in which the boundary is subdivided into a Dirichlet boundary ( $\Gamma_D$ ) and a Neumann boundary ( $\Gamma_N$ ) section. We consider the *steady-state groundwater flow equation*

$$\nabla \cdot (-K \nabla \phi) = \tilde{w}_{\text{inj}} - \tilde{w}_{\text{ext}} \quad \text{in } \Omega \quad (1)$$

subject to the boundary conditions:

$$\begin{aligned} \phi &= \hat{\phi}_D & \text{on } \Gamma_D \\ \vec{n} \cdot (-K \nabla \phi) &= 0 & \text{on } \Gamma_N \end{aligned} \quad (2)$$

in which  $\vec{n}(\vec{x})$  is the unit outer normal vector,  $K(\vec{x}) > 0$  is the spatially variable, but locally

isotropic hydraulic conductivity  $[m/s]$ ,  $\phi(\vec{x})$  is the hydraulic head  $[m]$  and the source terms on the right hand side prescribe the rates (volumetric flux per unit volume  $[1/s]$ ) of injection and extraction wells  $W_{\text{inj}}, W_{\text{ext}} \subsetneq \Omega$ :

$$\begin{aligned} \tilde{w}_{\text{inj}}(\vec{x}) & \begin{cases} > 0 & \vec{x} \in W_{\text{inj}} \\ = 0 & \vec{x} \in \Omega \setminus W_{\text{inj}} \end{cases} \\ \tilde{w}_{\text{ext}}(\vec{x}) & \begin{cases} > 0 & \vec{x} \in W_{\text{ext}} \\ = 0 & \vec{x} \in \Omega \setminus W_{\text{ext}} \end{cases} \end{aligned} \quad (3)$$

This is an elliptic equation for which the coefficient  $K$  may be highly variable. The fluid motion is induced by the head distribution. The volumetric flux is given by Darcy's law:

$$\vec{q} = -K\nabla\phi \quad \text{in } \Omega. \quad (4)$$

$\vec{q}$  is sometimes called the Darcy velocity. It is related to the pore water velocity  $\vec{v}$  via  $\vec{q} = \theta\vec{v}$  where  $\theta$  is the porosity. We work with  $\vec{q}$  and the porosity  $\theta$  is supposed to be constant.

## 2.2 Subsurface solute transport

A conservative tracer used to track flow motion has no influence on the flow itself. Its concentration  $c(t, \vec{x})$   $[kg/m^3]$  is described by the transient convection-diffusion-reaction equation [Bear and Cheng, 2010]

$$\begin{aligned} \frac{\partial(\theta c)}{\partial t} + \text{div}(-\mathcal{D}\nabla c) + \vec{q} \cdot \nabla c &= \tilde{w}_{\text{inj}} \tilde{c}_{\text{inj}} - \tilde{w}_{\text{ext}} c \\ & \text{in } (0, T] \times \Omega \end{aligned} \quad (5)$$

in which  $\tilde{c}_{\text{inj}}(t, \vec{x})$  is the concentration at the injection well and

$$\mathcal{D} = \theta \mathcal{D}_S \quad (6)$$

is the dispersion tensor  $[m^2/s]$  given by [Scheidegger, 1961]:

$$\mathcal{D}_S = (\alpha_\ell - \alpha_t) \frac{\vec{v} \cdot \vec{v}^T}{\|\vec{v}\|_2} + \left( \alpha_t \|\vec{v}\|_2 + D_m \right) \mathbf{Id}, \quad (7)$$

where  $\alpha_\ell$  and  $\alpha_t$  are the longitudinal and transversal dispersivities  $[m]$ ,  $D_m$  is the molecular diffusion coefficient  $[m^2/s]$  and  $\mathbf{Id}$  is the identity matrix. For the transport equation, we distinguish three types of boundaries, inflow, outflow and characteristic boundary:

$$\begin{aligned} \Gamma_- &= \{ \vec{x} \in \partial\Omega : \vec{q}(\vec{x}) \cdot \vec{n}(\vec{x}) < 0 \} \\ \Gamma_+ &= \{ \vec{x} \in \partial\Omega : \vec{q}(\vec{x}) \cdot \vec{n}(\vec{x}) > 0 \} \\ \Gamma_0 &= \{ \vec{x} \in \partial\Omega : \vec{q}(\vec{x}) \cdot \vec{n}(\vec{x}) = 0 \} \end{aligned} \quad (8)$$

Tracer in a constant concentration may enter over a fixed time period  $T_{\text{inj}} > 0$  through the injection well or somewhere on the inflow boundary:

$$c(t, \vec{x}) = \hat{c}_D(\vec{x}) \quad \text{on } \Gamma_- \quad (9)$$

On the whole boundary  $\partial\Omega = \Gamma_- \cup \Gamma_+ \cup \Gamma_0$ , we assume that the flux is non-diffusive for convection dominant transport:

$$\vec{n} \cdot (-\mathcal{D}\nabla c) = 0 \quad \text{on } \Gamma_- \cup \Gamma_+ \cup \Gamma_0 \quad (10)$$

This implies the no-flux condition for impermeable boundaries:

$$\vec{n} \cdot (-\mathcal{D}\nabla c + \vec{q}c) = 0 \quad \text{on } \Gamma_0 \quad (11)$$

We are interested in the steady-state solution ( $\partial c / \partial t = 0$ ), or more adequately, in the zeroth or first order temporal moments of the resident concentration [Harvey and Gorelick, 1995]. In all these cases, the differential equation takes the form of the *steady-state convection-diffusion equation*:

$$\text{div}(-\mathcal{D}\nabla u + \tau \vec{q} u) + \mu u = \tilde{s} \quad \text{in } \Omega. \quad (12)$$

The reaction coefficient  $\mu \in \mathbb{R}$  may be used as a sink term within extraction wells. The source term  $\tilde{s}$  may be used to describe the behavior at the injection well. The boundary conditions read:

$$\begin{aligned} u &= \hat{u}_D \quad \text{on } \Gamma_- \\ \vec{n} \cdot (-\mathbf{D}\nabla u) &= 0 \quad \text{on } \partial\Omega \end{aligned} \quad (13)$$

For  $\mu' = \mu - \text{div}(\vec{q})$ , equation (12) can be written in non-conservative form as

$$\text{div}(-\mathbf{D}\nabla u) + \vec{q} \cdot \nabla u + \mu' u = \tilde{s} \quad \text{in } \Omega. \quad (14)$$

### 3 Discretizations

#### 3.1 Preliminary definitions

Let  $\{\mathcal{T}_{h_\nu}\}_{\nu \in \mathbb{N}}$  be a family of structured or adaptively refined meshes (comprised of axis parallel cuboidal cells) that we get from a successive refinement of an initially structured mesh. Each  $\mathcal{T}_{h_\nu}$  forms a partitioning of  $\Omega$  into  $n_\nu$  disjoint cells (mesh elements), this means

$$\begin{aligned} \mathcal{T}_{h_\nu} &= \{t_j^\nu\}_{j=0, \dots, n_\nu-1} \\ \bar{\Omega} &= \bigcup_{j=0}^{n_\nu-1} \bar{t}_j^\nu, \quad t_i^\nu \cap t_j^\nu = \emptyset \quad \forall i \neq j. \end{aligned} \quad (15)$$

The variable  $\nu$  indicates the refinement level. As refinement proceeds, the meshsize

$$h_\nu = \max_{t \in \mathcal{T}_\nu^*} \left\{ \max_{\vec{x}, \vec{y} \in t} \|\vec{x} - \vec{y}\| \right\} \quad (16)$$

tends to 0.  $\mathcal{T}_\nu^*$  is understood to be the subset of  $\mathcal{T}_{h_\nu}$  that contains only the finest level cells. To keep notation readable, we write  $h$  instead of  $h_\nu$ ,  $\mathcal{T}_h$  instead of  $\mathcal{T}_{h_\nu}$  and  $n$  instead of  $n_\nu$  when it is clear or irrelevant which refinement level  $\nu$  we are considering.

The hydraulic conductivity is resolved on the structured mesh  $\mathcal{T}_{h_0}$ . It is described by a cell-wise constant function:

$$\begin{aligned} K_h(\vec{x}) &= K(\vec{x}_t) = \exp(Y(\vec{x}_t)) \\ \forall \vec{x} \in t, \vec{x}_t \text{ is the center the cell } t \in \mathcal{T}_{h_0}. \end{aligned} \quad (17)$$

Inside the wells, the hydraulic conductivity is supposed to be very high:

$$\begin{aligned} K_h(\vec{x}) &= 1.0 \quad \forall \vec{x} \in t, t \in \mathcal{T}_{h_0} \text{ with} \\ & \quad t \cap W_{\text{inj}} \neq \emptyset \quad \text{or} \quad t \cap W_{\text{ext}} \neq \emptyset. \end{aligned} \quad (18)$$

The hydraulic head distribution and the Darcy velocity (4) are computed on the same mesh. The transport equation (12), whose convective part is prescribed by the Darcy velocity, may be solved either on the same mesh or on a hierarchy of adaptively refined meshes based on  $\mathcal{T}_{h_0}$ ,

i.e. a cell of a subsequently refined mesh  $\mathcal{T}_{h_{\nu+1}}$  is always a subset of a cell in  $\mathcal{T}_{h_\nu}$ .

In our practical application, the estimated hydraulic conductivity fields have the smoothness of a Gaussian variogram model. The meshsizes are chosen in such a way that they resolve the correlation lengths well. Thus, the flow field on the mesh  $\mathcal{T}_{h_0}$  can be regarded as sufficiently accurate and we consider adaptive mesh refinement only for the solution of the transport problem. Finite elements on cuboids  $t \in \mathcal{T}_h$  are based on the polynomial space

$$\mathbb{Q}_k^d = \left\{ p(\vec{x}) = \sum_{\substack{0 \leq \alpha_i \leq k \\ 1 \leq i \leq d}} \gamma_{\alpha_1, \dots, \alpha_d} \cdot x_1^{\alpha_1} \cdots x_d^{\alpha_d}, \right. \\ \left. \vec{x} \in t \right\} \quad (19)$$

with maximal degree  $k$  in each coordinate direction. Discontinuous Galerkin (DG) approximations are based on the broken polynomial space

$$\begin{aligned} W_{h,k} &= W_{h,k}(\Omega, \mathcal{T}_h) = \left\{ u \in L^2(\Omega) : u|_t \in \mathbb{Q}_k^d \right. \\ & \quad \left. \forall t \in \mathcal{T}_h \right\}. \end{aligned} \quad (20)$$

We restrict ourselves to the case where the maximal polynomial degree  $k$  is constant for all cells:

$$\dim(W_{h,k}) = n \cdot \dim(\mathbb{Q}_k^d) = n \cdot (k+1)^d. \quad (21)$$

The continuous polynomial space

$$\begin{aligned} V_h &= V_h(\Omega, \mathcal{T}_h) = \left\{ u \in C^0(\bar{\Omega}) : u|_t \in \mathbb{Q}_1^d \right. \\ & \quad \left. \forall t \in \mathcal{T}_h \right\} \end{aligned} \quad (22)$$

is used to describe the standard Galerkin FEM and the streamline diffusion method. For a structured mesh with  $n = \prod_{i=1}^d n_i$  cells, its dimension is  $\prod_{i=1}^d (n_i + 1)$ .

All cell-wise or face-wise defined integrals that will occur in the following numerical schemes are integrals over products of at least two polynomials of order  $k$ . A Gaussian quadrature rule of order  $k + 1$  guarantees the exact evaluation of polynomials of order  $2k + 1$ .

### 3.2 FEM / SDFEM

Let  $V_h^0 = \{u \in V_h : u|_{\partial\Omega} = 0\}$  and assume  $\widehat{\phi}_D$  to be a piecewise linear approximation of the Dirichlet b.c. in (2). The standard Galerkin **FEM method** (cf. [Elman et al., 2005]) for solving (1)&(2) reads:

Find  $\phi_h \in V_h^D = \{u \in V_h : u|_{\Gamma_D} = \widehat{\phi}_D\}$  such that

$$\sum_{t \in \mathcal{T}_h} (K_h \nabla \phi_h, \nabla v_h)_{0,t} = \tilde{w}_h(v_h) \quad \forall v_h \in V_h^0. \quad (23)$$

The discrete source term on the right-hand side is

$$\begin{aligned} \tilde{w}_h(v_h) = & \sum_{\substack{t \in \mathcal{T}_h \\ t \cap W_{\text{inj}} \neq \emptyset}} (\tilde{w}_{\text{inj}}, v_h)_{0,t} \\ & - \sum_{\substack{t \in \mathcal{T}_h \\ t \cap W_{\text{ext}} \neq \emptyset}} (\tilde{w}_{\text{ext}}, v_h)_{0,t} \end{aligned} \quad (24)$$

where  $K_h \in W_{h_0,0}$  as defined in (17). The discrete Darcy velocity can be computed by direct pointwise evaluation of gradients of the polynomial basis on each cell  $t \in \mathcal{T}_{h_0}$ :

$$\vec{q}_h = -K_h \nabla \phi_h. \quad (25)$$

The **SDFEM method** (cf. [Brooks and Hughes, 1982]) for solving (14) reads:

Find  $u_h \in V_h^- = \{u \in V_h : u|_{\Gamma^-} = \widehat{u}_D\}$  such that

$$\begin{aligned} & \sum_{t \in \mathcal{T}_h} \left\{ (\mathbf{D} \nabla u_h, \nabla v_h)_{0,t} \right. \\ & \left. + (\vec{q}_h \nabla u_h + \mu'_h u_h, v_h + \delta_t^{\text{SD}} \cdot \vec{q}_h \nabla v_h)_{0,t} \right\} \\ & = \sum_{t \in \mathcal{T}_h} \left\{ (\tilde{s}_h, v_h + \delta_t^{\text{SD}} \cdot \vec{q}_h \nabla v_h)_{0,t} \right\} \\ & \quad \forall v_h \in V_h^0. \end{aligned} \quad (26)$$

$\mu'_h$  and  $\tilde{s}_h$  evaluate the corresponding terms of equation (14) at quadrature points. The matrix  $\mathbf{D} \in \mathbb{R}^{d \times d}$  is the discretized version of the dispersion tensor  $\mathcal{D}$  in (6) which is depending on  $\vec{v} = \vec{q}_h / \theta$ . The **stabilization parameter** determined by

$$\delta_t^{\text{SD}} = \frac{h}{2 \|\vec{q}_h\|_2} \cdot \zeta(\mathcal{P}_h^t) \quad (27)$$

is used to tune the amount of artificial diffusion depending on the magnitude of the **mesh Péclet number**  $\mathcal{P}_h^t$ . If  $\mathbf{D} = \varepsilon \cdot \mathbf{Id}$  ( $\varepsilon > 0$ ), the general definition of the mesh Péclet number is

$$\mathcal{P}_h^t = \frac{1}{2} \cdot \frac{\|\vec{q}_h\|_2 \cdot h_t}{\varepsilon}. \quad (28)$$

For the Scheidegger dispersion tensor (7), the effective mesh Péclet number according to [Cirpka and Kitanidis, 2001] is

$$\mathcal{P}_h^t = \frac{1}{2} \cdot \frac{\|\vec{q}_h\|_2 \cdot h_t}{\alpha \ell \cdot \|\vec{q}_h\|_2 + \theta D_m}. \quad (29)$$

There is a large variety of definitions for the function  $\zeta$  in the literature. The original choice in [Brooks and Hughes, 1982] is

$$\zeta(\mathcal{P}_h^t) = \coth(\mathcal{P}_h^t) - 1/\mathcal{P}_h^t. \quad (30)$$

We go for the more efficient approximation (cf. [Elman et al., 2005])

$$\zeta(\mathcal{P}_h^t) = \max \{ 0, 1 - 1/\mathcal{P}_h^t \}. \quad (31)$$

### 3.3 CCFV / DG

#### 3.3.1 Preliminary definitions

The following notation is inspired by the presentation of [Ern et al. \[2008\]](#). For a given mesh  $\mathcal{T}_h$ , each cell  $t \in \mathcal{T}_h$  has a cell-center  $\vec{x}_t$  and a  $d$ -dimensional cell-volume  $|t|$ . Given two neighboring cells  $t^-$  and  $t^+$  in  $\mathcal{T}_h$ , an interior face or interface  $f$  is defined as the intersection of their boundaries  $\partial t^- \cap \partial t^+$ . To be more precise, we write  $t_f^- = t^-$  and  $t_f^+ = t^+$ . The **unit normal vector**  $\vec{n}_f$  to  $f$  is assumed to be oriented from  $t_f^-$  to  $t_f^+$ . In the same manner,  $f$  is called a boundary face if there exists a  $t \in \mathcal{T}_h$  such that  $f = \partial t \cap \partial \Omega$  and we write  $t_f^- = t$ . In this case,  $\vec{n}_f$  is chosen to be the unit outer normal to  $\partial \Omega$ . We denote by  $\mathcal{E}_h$  the **set of interior faces** and by  $\mathcal{B}_h$  the **set of boundary faces**. For a face  $f \in \mathcal{E}_h \cup \mathcal{B}_h$ , we denote by  $\vec{x}_f$  its midpoint (face center), whereas  $\vec{x}_{f-}$  is the center of the cell  $t_f^-$ . For  $f \in \mathcal{E}_h$ , we denote by  $\vec{x}_{f+}$  the center of  $t_f^+$ .  $|f|$  is the  $(d-1)$ -dimensional volume of the face  $f$ .

A function  $u \in W_{h,k}$  is in general double valued on internal faces  $f \in \mathcal{E}_h$ . There, we set

$$u_f^\pm(\vec{x}) = \lim_{\varepsilon \rightarrow 0^\pm} u(\vec{x} + \varepsilon \vec{n}_f) \quad \vec{x} \in f. \quad (32)$$

The jump across  $f$  and the arithmetic mean value on  $f$  are given by

$$[[u]]_f = u_f^- - u_f^+ \quad \text{and} \quad \langle u \rangle_f(\vec{x}) = \frac{1}{2} (u_f^- + u_f^+) \quad (33)$$

respectively. Following convention, the definition of these terms is extended to the boundary  $\partial \Omega$  by:

$$[[u]]_f(\vec{x}) = \langle u \rangle_f(\vec{x}) = u(\vec{x}) \quad \forall \vec{x} \in f, \quad f \in \mathcal{B}_h. \quad (34)$$

We will suppress the letter  $f$  in subscripts if there is no ambiguity.

#### 3.3.2 Two-point flux cell-centered finite volume method (CCFV)

Using the function space  $W_{h,0}$ , the approximation of the boundary value problem (1) & (2) is

defined as follows:

Find  $\phi_h \in W_{h,0}$  such that

$$a^{\text{FV}}(\phi_h, v_h) = \ell^{\text{FV}}(v_h) \quad \forall v_h \in W_{h,0}. \quad (35)$$

The bilinear form  $a^{\text{FV}} : W_{h,0} \times W_{h,0} \rightarrow \mathbb{R}$  is defined by

$$a^{\text{FV}}(\phi, v) = \sum_{f \in \mathcal{E}_h} q_h^\phi(\vec{x}_f) \cdot [[v]]_f \cdot |f| + \sum_{f \in \mathcal{B}_h \cap \Gamma_D} q_h^\phi(\vec{x}_f) \cdot v(\vec{x}_{f-}) \cdot |f| \quad (36)$$

where

$$q_h^\phi(\vec{x}_f) := \begin{cases} -K_h^{\text{eff}}(\vec{x}_{f+}, \vec{x}_{f-}) \cdot \frac{\phi(\vec{x}_{f+}) - \phi(\vec{x}_{f-})}{\|\vec{x}_{f+} - \vec{x}_{f-}\|_2} & \text{for } f \in \mathcal{E}_h, \\ -K_h(\vec{x}_{f-}) \cdot \frac{\hat{\phi}_D(\vec{x}_f) - \phi(\vec{x}_{f-})}{\|\vec{x}_f - \vec{x}_{f-}\|_2} & \text{for } f \in \mathcal{B}_h \cap \Gamma_D. \end{cases} \quad (37)$$

is a two-point finite difference approximation of the normal component  $\vec{q} \cdot \vec{n}_f(\vec{x}_f)$  of the Darcy velocity  $\vec{q} = -K \nabla \phi$  through the face  $f$ . The discrete hydraulic conductivity  $K_h \in W_{h,0}$  is defined as in (17) and

$$K_h^{\text{eff}}(\vec{x}_{f+}, \vec{x}_{f-}) = \frac{2 \cdot K_h(\vec{x}_{f+}) \cdot K_h(\vec{x}_{f-})}{K_h(\vec{x}_{f+}) + K_h(\vec{x}_{f-})} \quad (38)$$

is the **harmonic average** of  $K_h(\vec{x}_{f+})$  and  $K_h(\vec{x}_{f-})$ . In the definition (37), we make use of the fact that the face  $f$  is perpendicular to the line connecting  $\vec{x}_{f+}$  and  $\vec{x}_{f-}$ .

The linear functional  $\ell^{\text{FV}} : W_{h,0} \rightarrow \mathbb{R}$  is given by

$$\begin{aligned} \ell^{\text{FV}}(v) = & \sum_{\substack{t \in \mathcal{T}_h \\ t \cap W_{\text{inj}} \neq \emptyset}} \tilde{w}_{\text{inj}}(\vec{x}_t) \cdot v(\vec{x}_t) \cdot |t| \\ & - \sum_{\substack{t \in \mathcal{T}_h \\ t \cap W_{\text{ext}} \neq \emptyset}} \tilde{w}_{\text{ext}}(\vec{x}_t) \cdot v(\vec{x}_t) \cdot |t| \end{aligned} \quad (39)$$

This approximation yields a cell-wise constant solution for which the Dirichlet boundary values  $\hat{\phi}_D$  are satisfied weakly.

### 3.3.3 Flux reconstruction

So far, only the normal flux component  $q_h^\phi(\vec{x}_e)$  from (37) is available on the midpoints of the faces of a cell  $t \in \mathcal{T}_h$ . But we need to evaluate the Darcy velocity on internal points of a cell. The simplest  $H(\text{div})$ -conforming flux reconstruction is achieved using Raviart-Thomas elements of order 0 [Brezzi and Fortin, 1991; Raviart and Thomas, 1977],

$$\mathbb{RT}_0(t) = \left\{ \vec{\tau}(\vec{x}) : \begin{aligned} & \tau_i = a_i + b_i x_i, \quad \vec{x} \in t, \\ & 1 \leq i \leq d, \quad a_i, b_i \in \mathbb{R} \text{ fixed} \end{aligned} \right\}, \quad (40)$$

for which the polynomial space is defined by

$$\mathbb{RT}_0(\Omega, \mathcal{T}_h) = \left\{ \vec{\tau} \in [L^2(\Omega)]^d : \vec{\tau}|_t \in \mathbb{RT}_0(t) \quad \forall t \in \mathcal{T}_h \right\}. \quad (41)$$

The discrete Darcy velocity

$$\vec{q}_h \in \mathbb{RT}_0(\Omega, \mathcal{T}_h) \quad (42)$$

can be evaluated component-wise by a linear interpolation between the normal fluxes on opposing face midpoints. It can be shown that the reconstructed Darcy velocity  $\vec{q}_h \in \mathbb{RT}_0(\Omega, \mathcal{T}_h)$  is

indeed in  $H(\text{div}, \Omega)$  and satisfies the projection condition:

$$\int_f (\vec{q}_h - \vec{q}) \cdot \vec{n}_f \, ds = 0 \quad (43)$$

Compared to the direct evaluation (25), this reconstructed Darcy velocity field is pointwise divergence-free if the groundwater equation (1) is free of any source or sink terms ( $\tilde{w}_{\text{inj}} = \tilde{w}_{\text{ext}} = 0$ ).

### 3.3.4 Discontinuous Galerkin method (DG)

The symmetric weighted interior penalty (SWIP) method presented in [Ern et al., 2008] is a robust discontinuous Galerkin method accounting for anisotropy and discontinuity in the diffusion tensor of (12).

For the discretization of the diffusive term, the authors have introduced a scalar- and double-valued weighting function  $\omega$  on internal faces. The two values  $\omega^-$  and  $\omega^+$  are constructed based on the double-valued diffusion tensor  $\mathbf{D}$  with  $\mathbf{D}^-$  and  $\mathbf{D}^+$  defined element-wise following (32). Using the normal component of  $\mathbf{D}^\mp$  across the face, namely  $\delta^\mp = \vec{n}_f \cdot \mathbf{D}^\mp \cdot \vec{n}_f$ , the weighting factors are defined as

$$\omega^- = \frac{\delta^+}{\delta^- + \delta^+} \quad \text{and} \quad \omega^+ = \frac{\delta^-}{\delta^- + \delta^+}. \quad (44)$$

Both factors are non-negative and add up to unity  $\omega^- + \omega^+ = 1$ .

For  $v \in W_{h,k}$ , the weighted average of the diffusive flux is defined as

$$\langle \mathbf{D}\nabla v \rangle^\omega = \omega^- (\mathbf{D}\nabla v)^- + \omega^+ (\mathbf{D}\nabla v)^+. \quad (45)$$

On the boundary face  $f \in \mathcal{B}_h$ , we set  $\omega = 1$  and  $\langle \mathbf{D}\nabla v \rangle^\omega = \mathbf{D}\nabla v$ .

For the convective term, we choose an **upwind flux** formulation that is equivalent to the presentations in [Georgoulis et al., 2009], in §4.2 of [Rivière, 2008] or in §4.6.2 of [Pietro and Ern, 2012]. For an internal face  $f \in \mathcal{E}_h$  lying between two neighboring cells  $t_f^-$  and  $t_f^+$ , recall that the unit normal vector  $\vec{n}_f$  is assumed to be oriented from  $t_f^-$  to  $t_f^+$ . For a boundary face  $f \in \mathcal{B}_h$ ,  $\vec{n}_f$

is the unit outer normal. By  $u^{\text{upwind}}$  we denote the upwind value of a function  $u \in W_{h,k}$ . For  $\vec{x} \in f, f \subset \partial t \setminus \Gamma_-$ , it is defined by

$$u^{\text{upwind}}(\vec{x}) = \begin{cases} u^+(\vec{x}) & \text{if } \vec{q}_h(\vec{x}) \cdot \vec{n}_f < 0 \\ u^-(\vec{x}) & \text{if } \vec{q}_h(\vec{x}) \cdot \vec{n}_f \geq 0 \end{cases}$$

The higher order DG approximation<sup>1</sup> of the boundary value problem (12)&(13) reads:

Find  $u_h \in W_{h,k}$  such that

$$a^{\text{DG}}(u_h, v_h) = \ell^{\text{DG}}(v_h) \quad \forall v_h \in W_{h,k}. \quad (46)$$

The bilinear form is defined by

$$\begin{aligned} a^{\text{DG}}(u, v) = & \sum_{t \in \mathcal{T}_h} \left\{ (\mathbf{D}\nabla u, \nabla v)_{0,t} - (u, \vec{q}_h \cdot \nabla v)_{0,t} + (\mu_h u, v)_{0,t} \right\} \\ & \text{(cell terms)} \\ & + \sum_{f \in \mathcal{E}_h} \left\{ (\gamma \llbracket u \rrbracket, \llbracket v \rrbracket)_{0,f} + (|\vec{n}_f \cdot \vec{q}_h| u^{\text{upwind}}, \llbracket v \rrbracket)_{0,f} \right. \\ & \left. - (\langle \vec{n}_f \cdot \mathbf{D}\nabla u \rangle^\omega, \llbracket v \rrbracket)_{0,f} - (\langle \vec{n}_f \cdot \mathbf{D}\nabla v \rangle^\omega, \llbracket u \rrbracket)_{0,f} \right\} \\ & \text{(interior face fluxes)} \\ & + \sum_{f \in \mathcal{E}_h \cap \Gamma_+} (\vec{n}_f \cdot \vec{q}_h u, v)_{0,f} \\ & \text{(convective outflow)} \\ & + \sum_{f \in \mathcal{B}_h \cap \Gamma_-} \left\{ (\gamma(u - \widehat{u}_D), v)_{0,f} \right. \\ & \left. - (u - \widehat{u}_D, \vec{n}_f \cdot \mathbf{D}\nabla v)_{0,f} \right\} \\ & \text{(Dirichlet B.C.)} \end{aligned} \quad (47)$$

The linear functional is given by

$$\begin{aligned} \ell^{\text{DG}}(v) = & \sum_{t \in \mathcal{T}_h} (\bar{s}_h, v)_{0,t} \\ & - \sum_{f \in \mathcal{B}_h \cap \Gamma_-} (\vec{n}_f \cdot \vec{q}_h \widehat{u}_D, v)_{0,f} \end{aligned} \quad (48)$$

*(source term and Dirichlet B.C.)*

<sup>1</sup> DG( $k$ ) indicates that the polynomial basis is from  $\mathbb{Q}_k^d$ . The colors in the following terms are red for the convection terms, blue for the diffusion terms, green for the reaction term and grey for the source term.

$\mu_h$  and  $\bar{s}_h$  evaluate the corresponding terms of equation (12) at quadrature points. The parameter  $\gamma$  penalizing discontinuity in the solution is given in [Bastian, 2011] by

$$\gamma = C_\gamma \cdot \frac{D_{\text{eff}} \cdot k(k+d-1)}{h_f} \quad (49)$$

$\forall f \in \mathcal{E}_h \cup (\mathcal{B}_h \cap \Gamma_-)$

where  $C_\gamma > 0$  is a constant to be chosen sufficiently large ( $C_\gamma = 10$  is usually enough). With this definition of  $\gamma$  the user-chosen constant does not play a big role anymore in the convection-dominated case.

Remember that for the discrete problem (46),  $\mathcal{T}_h$  can be a non-conformingly refined cuboidal mesh. For a face lying between two possibly non-matching elements, we set  $h_f = \min\{h_f^-, h_f^+\}$  where  $h_f^\mp = \text{diam}(f \cap \partial t_\mp)$  are face diameters. On internal faces, the effective diffusivity is defined by the harmonic average

$$D_{\text{eff}} = \frac{2\delta^-\delta^+}{\delta^- + \delta^+} \quad (50)$$

of the normal component of the diffusion tensor across the face. On boundary faces, we set directly

$$D_{\text{eff}} = \vec{n}_f \cdot \mathbf{D} \cdot \vec{n}_f. \quad (51)$$

## 4 Adaptive mesh refinement

We are interested in reducing numerical oscillations globally. Adaptive mesh refinement is a particularly promising way of achieving this goal.

Residual-based a-posteriori error estimators offer the advantage of small evaluation cost because they are based on local residual terms. We consider two existing  $h$ -adaptive versions for the above mentioned discretization schemes of the transport problem. Let  $u_h$  be the SDFEM solution (26) or the DG solution (46) respectively. The residual-based error estimator described by Verfürth [1998, 2005], developed for the finite element and the SDFEM discretization of the steady-state convection-diffusion equation, is based on the following local error indicator:

For each element  $t \in \mathcal{T}_h$ , the local error indicator  $\eta_t^2$  is given by the sum of two terms,

$$\eta_t^2 = \eta_{R_t}^2 + \eta_{R_f}^2, \quad (52)$$

an element residual term<sup>2</sup>

$$\eta_{R_t}^2 = \frac{h_t^2}{\varepsilon} \left\| s_h + \varepsilon \Delta u_h - \vec{q}_h \cdot \nabla u_h - \mu'_h u_h \right\|_{L^2(t)}^2 \quad (53)$$

and a face residual term

$$\eta_{R_f}^2 = \frac{1}{2} \sum_{f \in \partial t \setminus \Gamma} \frac{h_f}{\varepsilon} \left\| \llbracket \vec{n} \cdot (\varepsilon \nabla u_h) \rrbracket \right\|_{L^2(f)}^2.$$

To these two terms, [Schötzau and Zhu \[2009\]](#) added a third term measuring jumps of the solution on internal or inflow boundary faces

$$\begin{aligned} \eta_{J_f}^2 &= \frac{1}{2} \sum_{f \in \partial t \setminus \Gamma} \left( \frac{\gamma \varepsilon}{h_f} + \frac{h_f}{\varepsilon} \right) \left\| \llbracket u_h \rrbracket \right\|_{L^2(f)}^2 \\ &+ \sum_{f \in \partial t \cap \Gamma_-} \left( \frac{\gamma \varepsilon}{h_f} + \frac{h_f}{\varepsilon} \right) \left\| (u_h - \hat{u}_D) \right\|_{L^2(f)}^2 \end{aligned}$$

to construct a residual-based error estimator for the interior penalty DG discretization scheme. Hence, the local error indicator  $\eta_t^2$  for each element  $t \in \mathcal{T}_h$  is given by the sum of three terms,

$$\eta_t^2 = \eta_{R_t}^2 + \eta_{R_f}^2 + \eta_{J_f}^2. \quad (54)$$

In our concrete application, we choose  $\varepsilon = \min_{1 \leq i \leq d} \{\mathbf{D}_{ii}\}$  to avoid underestimation.

The a-posteriori error estimator (in both cases) is defined by

$$\eta = \left( \sum_{t \in \mathcal{T}_h} \eta_t^2 \right)^{1/2}. \quad (55)$$

Schötzau and Zhu have shown that their error estimator is robust in convection-dominated regimes, effective in locating characteristic and boundary layers and that the error in the energy norm converges with optimal order as soon as

<sup>2</sup>Note that  $\Delta u_h$  can be omitted for the polynomial degree  $k = 1$ .

refinement reaches a state when the local mesh Péclet number is of order 1. An extension to  $hp$ -adaptivity can be found in [\[Zhu and Schötzau, 2011\]](#). The performance of Verfürth's error estimator is assessed in a comparative study by [John \[2000\]](#).

Alternative error estimators for DG discretization schemes of the convection-diffusion equation can be found in [\[Ern et al., 2010\]](#) and [\[Georgoulis et al., 2009\]](#).

A robust error estimator is one aspect of adaptivity. Another important aspect is a marking strategy that achieves an equitable distribution of error contributions. An error-fraction based refinement strategy has the following characteristics: Given a fixed refinement fraction  $p_r$  [%] and the list of all cells sorted by the magnitude of the local error indicators

$$\eta_{t_{j_1}}^2 \leq \eta_{t_{j_2}}^2 \leq \dots \leq \eta_{t_{j_n}}^2,$$

the goal is to mark the cells with the largest local errors for refinement such that their contribution to the total error is  $p_r$  [%]. To be more precise, we need to find the largest  $\eta^*$  such that

$$\sum_{t \in \mathcal{T}_h: \eta_t \geq \eta^*} \eta_t^2 \geq \frac{p_r}{100} \cdot \eta^2 \quad (56)$$

using the bisection method and mark the top contributors  $t \in \mathcal{T}_h$  with  $\eta_t \geq \eta^*$  for refinement. This strategy is readily parallelizable: the sum on the left hand side of (56) and the total error  $\eta^2$  get their contributions from all processes. The very same strategy can be used to mark the mesh cells with the lowest error contribution for coarsening, given a fixed coarsening fraction  $p_c$  [%]: Find the smallest  $\rho^*$  such that

$$\sum_{t \in \mathcal{T}_h: \eta_t \leq \rho^*} \eta_t^2 \leq \frac{p_c}{100} \cdot \eta^2 \quad (57)$$

and mark all cells  $t \in \mathcal{T}_h$  for which  $\eta_t \leq \rho^*$  for coarsening. Note that the choice of the fixed parameters  $p_r$  and  $p_c$  are dependent on the error distribution and have a strong influence on the efficiency of the scheme.

For higher order polynomials, the second order derivative in the element residual term (53) would be required. In the small 2-D test problems, this is neglected. In the solute transport simulations, we apply adaptivity only to the DG(1) discretization. For a comparative study based on small 2-D test problems, a sequential version of the adaptive SDFEM code is sufficient. Remember that in the practical application,  $\mathcal{T}_0$  is the mesh on which

- the conductivity field  $K$  is resolved (17),
- the flow equation (1) is solved as in §3.3.2 and
- the Darcy flux (4) is evaluated as in §3.3.3.

The mesh  $\mathcal{T}_0$  should be sufficiently fine such that the main features of the solution are visible and a partitioning of the mesh among all available processes is possible. The **stopping criterion** for refinement is reached as soon as either of the following conditions is fulfilled:

- (i) The estimated error is below some prescribed tolerance:  $\eta \leq TOL$ .
- (ii) Provided that the range of the true solution  $u$  is given by  $[0, \hat{u}]$ , we may choose a tolerance of  $p_{osc} = 5\%$  for the maximal under- and overshoots by

$$\max \left\{ \frac{|u_{\min}|}{\hat{u}}, \frac{u_{\max} - \hat{u}}{\hat{u}} \right\} < p_{osc}. \quad (58)$$

- (iii) The mesh refinement level  $L$  or the total number of unknowns has exceeded a certain limit.

The  **$h$ -adaptive mesh refinement algorithm** for the solution of the convection-diffusion equation can be formulated as follows.

---

**Algorithm 1**  $h$ -adaptive refinement

---

**Input:** Appropriate values for  $p_r$  and  $p_c$ .

- (1) Start with mesh level  $L = 0$ .
- (2) Compute the solution  $u_{h_0}$  of (46) on  $\mathcal{T}_{h_0}$ .
- (3) Compute the error estimator  $\eta$  as in (55) for  $u_0$ .

**while**  $\eta > TOL$  **do**

- (4) Apply the marking strategy (56).
- (5) Refine the mesh and set  $L = L + 1$ .

**if**  $L > L_{\max}$  **then**

break; ▷ // maximal number of refinement steps exceeded

**end if**

(2') Compute the solution  $u_{h_L}$  of (46) on  $\mathcal{T}_{h_L}$ .

**if** (58) holds **then**

break; ▷ // overshoots and undershoots are small enough

**end if**

(3') Compute the error estimator  $\eta$  as in (55) for  $u_{h_L}$ .

**end while**

**Output:**  $u_{h_L}$

---

In each refinement step, the linear system for (46) can be solved independently of solutions from the previous refinement step since the problem is linear and stationary.

## 5 Diffusive $L^2$ -projection

In this section, we present another method to reduce numerical oscillations. Due to its simplicity we consider this a post-processing step for the DG solution. Given the DG solution  $u_{DG} \in W_{h,k}$  on the coarse level  $h = h_0$ , our goal is to find an approximation of  $u_{DG}$  in the space  $V_h$  of continuous Galerkin finite elements that preserves the profile of the DG solution, but with a significant reduction of spurious oscillations. The  $L^2$ -projection is a good candidate. It is well-known to give a good on average approximation of a function and it does not require the approximated function to be continuous. Furthermore, an extra term imitating a small amount of

diffusive flux can be added. This way, the  $L^2$ -projection can be interpreted as the solution of a diffusion-reaction equation without boundary constraints. This leads to the following variational problem:

Find  $u_h \in V_h$  such that

$$\begin{aligned}
 (\varepsilon_h \nabla u_h, \nabla v_h)_{0,\Omega} + (u_h, v_h)_{0,\Omega} &= (u_{\text{DG}}, v_h)_{0,\Omega} \\
 \forall v_h \in V_h. &
 \end{aligned}
 \tag{59}$$

Hereby, we choose the extra diffusion  $\varepsilon_h = \frac{1}{2}h^2$  in such a way that the diffusivity of characteristic layers are in the order of magnitude of the meshsize  $\sim O(\sqrt{\varepsilon_h}) = O(h)$ .

## 6 Efficient solution of the arising linear systems

### 6.1 Flow equation and diffusive $L^2$ -projection

The linear systems arising from the discrete elliptic problems (23) or (35) and (59) are all of the size  $O(n^2)$ , symmetric positive definite and can be solved very efficiently using the combination CG with AMG. The AMG preconditioner described by Blatt [2010] is designed for the solution of problems of the type (1) with a highly discontinuous coefficient  $K$ .

### 6.2 Transport equation

By contrast, the stiffness matrix of the discrete transport equation is non-symmetric. BiCGSTAB or alternatively GMRES are used in our numerical tests. For the SDFEM discretization (26), the matrix size is also  $O(n^2)$ . In the more diffusive case of heat transport, parallel AMG may be used as a preconditioner. In the convection-dominated case, the SSOR or ILU(0) preconditioners are used.

As mentioned in the introduction, for the discretization of a first order hyperbolic problem using an upwind scheme, the order in which the unknowns are indexed, plays an important role

for the performance and stability of an iterative solver. The main purpose of ordering unknowns in flow direction can already be found in [Reed and Hill, 1973]. The downwind numbering algorithms described in the works of Bey and Wittum [1997] and Hackbusch and Probst [1997] handle arbitrary velocity fields. Steady-state groundwater flow (with a scalar conductivity field) is a potential flow and therefore always cycle-free. Since the velocity field is induced by the hydraulic head, the latter can be used directly as the sorting key for the unknowns.

For the DG discretization, it is advisable to collect the unknowns of the solution vector  $\vec{u}_h$  block-wise where each vector block  $\vec{u}^{(t)}$  holds the unknowns of  $\{u_1^{(t)}, \dots, u_{n_{\text{local}}}^{(t)}\}$  of a single mesh cell  $t$  with  $n_{\text{local}}$  denoting the dimension of the local polynomial space. The stiffness matrix  $\mathbf{A}_h$  becomes a block matrix with constant block-size  $n_{\text{local}} \times n_{\text{local}}$ . The arising linear system

$$\mathbf{A}_h \vec{u}_h = \vec{b}_h \tag{60}$$

is of the size  $O(n^2 \cdot n_{\text{local}}^2)$  and can be solved efficiently using a block version of BiCGSTAB or GMRES combined with SSOR or ILU(0) preconditioning, after a renumbering of mesh cells: In the hyperbolic limit the bilinear form of the DG discretization is reduced to the terms listed in the first two lines of (47). If the mesh cells are sorted according to the hydraulic head distribution  $\phi$  the stiffness matrix  $\mathbf{A}_h$  obtains the shape of a block-triangular matrix. In this case, the symmetric block Gauss-Seidel method for (60) becomes a direct solver because it converges after one step.

If the groundwater flow and the solute transport equations are solved on the same mesh, this procedure is straightforward. Otherwise, if adaptive refinement is applied only to the solution of the transport problem, as mentioned in subsection 3.1, the hydraulic head  $\phi$  must be reconstructed on the locally refined sub-cells. Given the discrete Darcy velocity  $\vec{q}_h$  in the form (42), the hydraulic head can be locally reconstructed

as a quadratic function

$$\tilde{\phi}|_t = \sum_{j=1}^d (a_j x_j^2 + b_j x_j) + c_0 \quad (61)$$

satisfying

$$\tilde{\phi}|_t = \phi|_t \quad (62)$$

on the cell center and the discrete form of Darcy's law

$$-K \nabla \tilde{\phi}|_t = \vec{q}_h \quad (63)$$

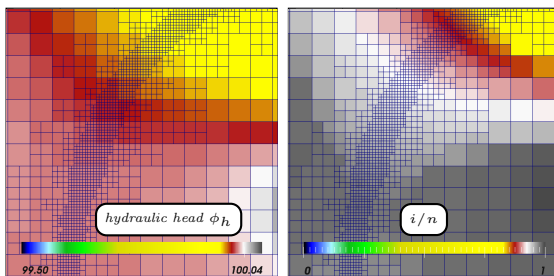


Figure 1: Downwind numbering of locally refined mesh cells: The hydraulic head  $\phi$  is constant on each coarse mesh cell (upper plot). For the renumbering of mesh cells according to the hydraulic head, it has to be resolved on the locally refined sub-cells. The cell index  $i$  in the lower plot is sorted according to  $\tilde{\phi}$ .  $n$  is the total number of all cells of the locally refined mesh.

on the  $2d$  face centers of a coarse mesh cell  $t \in \mathcal{T}_0$ . This yields  $2d+1$  equations for the  $2d+1$  coefficients of  $\tilde{\phi}|_t$ . The locally refined sub-cells can then be sorted according to  $\tilde{\phi}|_t$  evaluated at the centers of the sub-cells (Figure 1).

Due to the large problem size in 3-D, parallelization is necessary for efficiency. After each refinement step, the parallel partition-blocks<sup>3</sup> of the coarse mesh  $\mathcal{T}_0$  (and with it all locally refined sub-cells) may be altered to achieve a similar amount of refined sub-cells on every processor

<sup>3</sup> In general, the shape of these blocks are not cuboidal.

partition (**dynamic load-balancing**). To ensure that the renumbering procedure still works after each repartitioning step, the two quantities  $\phi$  and  $K$  have to

be made available on each processor partition of  $\mathcal{T}_0$  for a new reconstruction of  $\vec{q}_h$  and  $\tilde{\phi}$ .

## 7 Numerical Studies

In §7.1 and §7.2, we start with two singularly perturbed problems on the unit square for which analytical solutions exist in the domain of interest. Convergence tests can be performed using global and adaptive refinement. For the first problem, we demonstrate the influence of the ordering of unknowns on the performance of the iterative solvers for linear systems arising from a DG(1) discretization as described in section 6. The second problem has a less regular solution. In §7.3, we take a closer look on the quality of the diffusive  $L^2$ -projection compared to the SDFEM solution on a structured mesh. In §7.4 and §7.5, we show a 2-D and a 3-D example of the coupled groundwater flow and transport problem. Since analytical solutions are not available, numerical solutions computed on adaptively refined meshes are taken as reference solutions for assessing the quality of different solution methods computed on a coarse structured mesh.

For computations on structured meshes in 2-D and in 3-D, we use the YASP grid, an implementation of a structured parallel mesh available in the `dune-grid` module. For sequential adaptive refinement in 2-D, we use the UG grid [Bastian et al., 1997], and for parallel adaptive refinement with dynamic load-balancing in 3-D, we use the DUNE ALUGrid module [Dedner et al., 2014].

In all computations, the best available linear solver / preconditioner combination (in terms of robustness and speed) is chosen for each linear system arising from a finite element discretization of a stationary problem.

All time measurements are based on the **wall-clock time**, i.e. the difference between the time at which a certain task finishes and the start time

of that task. It may include time that passes while waiting for resources to become available.

All 2-D computations are performed in sequential mode on a laptop with an *Intel® Core™2 Duo CPU (P9500, 2.53 GHz)* and 4 GB total memory. All 3-D computations are performed on a multi-core architectures with large memory and high-speed network communication links. Table 6 give an overview of the used hardware.

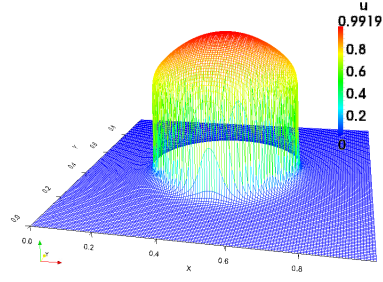


Figure 2: Profile of the analytical solution  $u$  for  $\varepsilon = 10^{-5}$ .

### Linear solver performance and accuracy

#### 7.1 An example with a regular solution

Let  $(x, y) \in \bar{\Omega} = [0, 1]^2$  and consider the boundary value problem (from [John et al., 1997])

$$-\varepsilon \Delta u + \vec{q} \cdot \nabla u + \mu \cdot u = \tilde{s}_\varepsilon \text{ in } \Omega \quad (64)$$

$$u = 0 \text{ on } \partial\Omega \quad (65)$$

where  $\vec{q} = (2, 3)^T$ ,  $\mu = 2$  and the source term  $\tilde{s}_\varepsilon(x, y)$  is chosen such that

$$u(x, y) = \frac{16}{\pi} x(1-x)y(1-y) \left( \frac{\pi}{2} + \arctan \left[ \frac{2}{\sqrt{\varepsilon}} \xi(x, y) \right] \right) \quad (66)$$

with

$$\xi(x, y) = 0.25^2 - (x - 0.5)^2 - (y - 0.5)^2. \quad (67)$$

For our tests, we choose  $\varepsilon = 10^{-5}$ . Note that in this example, the internal layer is generated by a source term which itself depends on  $\varepsilon$ . For  $\varepsilon \ll 1$ , an accurate representation of the source term requires a fine mesh, because, in a finite element discretization of  $\tilde{s}_\varepsilon$ , the error in the quadrature-rule might become dominating on a coarse mesh. Since we investigate the convergence behavior for global and adaptive refinement, this is not a severe problem.

$L$	$DOF$	random		horizontal		downstream		
		$IT$	$TIT[s]$	$IT$	$TIT[s]$	$IT$	$TIT[s]$	$T_{\text{sort}}[s]$
9	6,856	8	0.005	4	0.004	1	0.008	0.003
10	10,528	9	0.008	5	0.007	1	0.008	0.006
11	19,672	13	0.015	6	0.014	2	0.010	0.012
12	34,540	17	0.028	7	0.026	2	0.028	0.022
13	85,468	25	0.081	9	0.079	3	0.068	0.059
14	150,016	34	0.152	10	0.138	4	0.127	0.123
15	278,836	48	0.325	12	0.262	5	0.246	0.284
16	544,300	73	0.770	14	0.516	7	0.496	0.661

Table 1: Performance of the linear solver (BiCGSTAB + SSOR with reduction  $10^{-8}$ ) for different cell numbering strategies applied to the DG(1) method:  $L$  = refinement level,  $DOF$  = degrees of freedom,  $IT$  = number of iterations for the linear solver,  $TIT$  = time per iteration,  $T_{\text{sort}}$  = time for renumbering the grid cells.

Starting on a coarse structured mesh with  $h_0 = 1/8$ , we perform an adaptive refinement loop three times, based on three different ways of cell numbering as depicted in Figures 3(a)-(c). For the SDFEM discretization, the different cell numbering has no influence on the speed of the linear solver. For the DG(1) discretization, Table 1 confirms that an optimal numbering of degrees of freedom (following the velocity field) results

in a faster solution of the arising linear system. The time for renumbering the grid cells is comparable to the time for one step of the iterative linear solver.

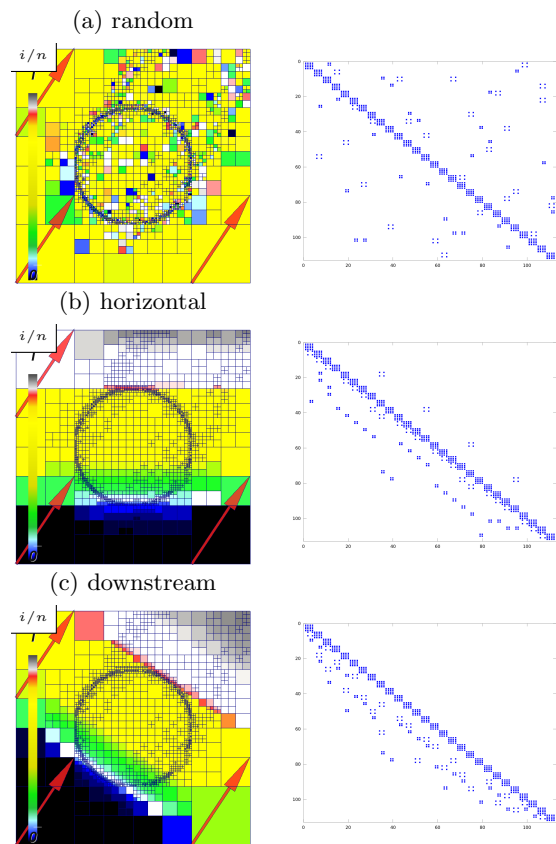


Figure 3: Different cell numbering strategies and corresponding matrix patterns for the DG(1) method. The block matrix for  $\mathbb{Q}_1$  elements in 2-D is made of  $4 \times 4$  - blocks.  $i =$  cell index,  $n =$  total number of mesh cells.

On coarse meshes, the matrix pattern can assume a block-triangular form (Figure 3(c)). In these cases, the iteration number is indeed 1. As refinement proceeds, the meshsizes and therefore the mesh Péclet numbers decrease and we diverge from the hyperbolic limit. Although this increases the iteration numbers, they stay at a

low level for the optimal numbering. Not only the number of iterations is reduced but also the required time per iteration. The linear solver used is BiCGSTAB with SSOR. Similar results are obtained with the combinations BiCGSTAB + ILU(0), GMRES + SSOR and GMRES + ILU(0).

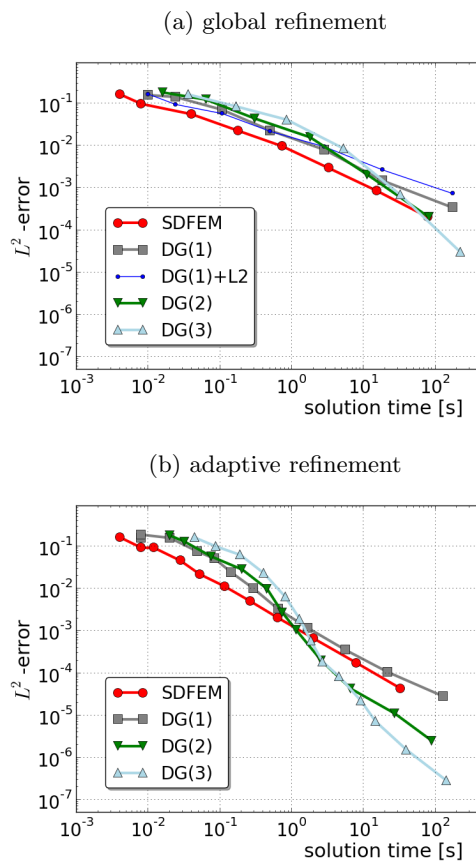


Figure 4: Example by John: (a) global refinement on a structured mesh and (b) adaptive refinement on an unstructured mesh (UG), both starting on a coarse mesh with meshsize  $h = 1/8$ . The refinement and coarsening fractions for the adaptive refinement algorithm are  $p_r = 95\%$  and  $p_c = 0.5\%$ . Linear solver used: BiCGSTAB + SSOR with reduction  $10^{-8}$ . Solution time = system assembly time + linear solver time.

We measure accuracy with respect to com-

puting time. The SDFEM method with bilinear elements is compared to the DG( $k$ ) methods (with globally constant polynomial degree  $k \in \{1, 2, 3\}$ ) in a convergence test with uniform and adaptive refinement. Accuracy is measured in the  $L^2$ -norm of the error taken over the domain of interest:  $\|u - u_h\|_{L^2(\Omega)}$ . The solution time is the sum of the system assembly time and the linear solver time. For the DG( $k$ ) methods, we apply an optimal numbering of mesh cells to speed up the linear solver. The time required to sort the mesh cells is negligible compared to the solution time.

The solution time is linearly proportional to the number of unknowns. For a comparable number of degrees of freedom (DOF), the iterative linear solvers perform better for the DG-based methods.

From Figure 4 we can make the following observations:

1. For the same computing time, SDFEM is more accurate than DG(1).
2. The accuracy of the higher order DG methods overtakes the accuracy of SDFEM at a certain refinement level. This happens as soon as the steep gradient is resolved and optimal convergence order is achieved.
3. With adaptive refinement, higher accuracy is achieved at an earlier stage.

The blue curve (DG(1)+L2) in the first plot displays the accuracy of the post-processed DG(1) solution on a structured mesh. Although it is close to the DG(1) curve, in this case, the diffusive  $L^2$ -projection adds an extra amount of error. Since solution time for the post-processing step is a small fraction of the solution time for the transport problem, it is neglected in this plot.

## 7.2 An example with a less regular solution

Let  $(x, y) \in [0, 1]^2$ . We consider the boundary value problem

$$-\varepsilon \Delta u + \vec{q} \cdot \nabla u = 0 \quad \text{in } [0, 1]^2 \quad (68)$$

with constant velocity  $\vec{q} = \frac{\sqrt{2}}{2}(1, 1)^T$  and discontinuous boundary conditions

$$u(x, 0) = 1 \quad \text{and} \quad u(0, y) = 0. \quad (69)$$

Obviously, the solution has a jump at the origin and is therefore not  $H^1$ -regular. This jump causes a characteristic boundary layer along the direction  $\vec{q}$ . This example is close to a real-world example in the sense that the discontinuity may be used to describe a binary state and the direction of the velocity is not aligned to the mesh. Theorem 1 of [López and Sinusía, 2004] provides an asymptotic expansion of the solution  $u$  on the subset  $\Omega = [0, 1]^2 \setminus \mathbf{U}_0$  where  $\mathbf{U}_0 = \{\vec{y} \in \mathbb{R}^2 : \|\vec{y}\|_2 < r_0\}$  is a ball with radius  $r_0 > 0$  and center  $(0, 0)$ . Introducing polar coordinates through  $x = r \sin \varphi$  and  $y = r \cos \varphi$ , we get

$$u = u_0(r, \varphi) + \frac{e^{wr(\sin(\varphi+\beta)-1)}}{\pi\sqrt{2wr}} u_1(r, \varphi) \quad (70)$$

where  $\beta = \pi/4$ ,  $w = \|\vec{q}\|_2/(2\varepsilon)$  and

$$u_0(r, \varphi) = \frac{1}{2} \begin{cases} \operatorname{erfc}\left(\sqrt{(1-\sin(\varphi+\beta))wr}\right) & \text{if } \varphi < \beta, \\ 1 & \text{if } \varphi = \beta, \\ 2 - \operatorname{erfc}\left(\sqrt{(1-\sin(\varphi+\beta))wr}\right) & \text{if } \varphi > \beta. \end{cases} \quad (71)$$

The function  $u_1(r, \varphi)$  has an asymptotic expansion from which we use only the first term,

$$u_1(r, \varphi) = \begin{cases} \Gamma(1/2) \left\{ \left( \frac{\cos(\varphi-\beta)}{\cos(\varphi+\beta)} - \frac{\cos(\varphi+\beta)}{\cos(\varphi-\beta)} \right) - \frac{1}{2 \sin(\frac{1}{2}(\frac{\pi}{2} - \varphi - \beta))} \right\} & \text{if } \varphi \neq \pi/4, \\ 0 & \text{if } \varphi = \pi/4, \end{cases} \quad (72)$$

hereby neglecting higher order terms of  $\varepsilon$ .

For our tests, we choose  $\varepsilon = 10^{-5}$  and  $r_0 = 5 \times 10^{-5}$ . The small area  $\mathbf{U}_0(r_0)$  around the critical

location  $(0,0)$ , where the numerical errors are largest and a different asymptotic expansion is necessary, is left out of consideration.

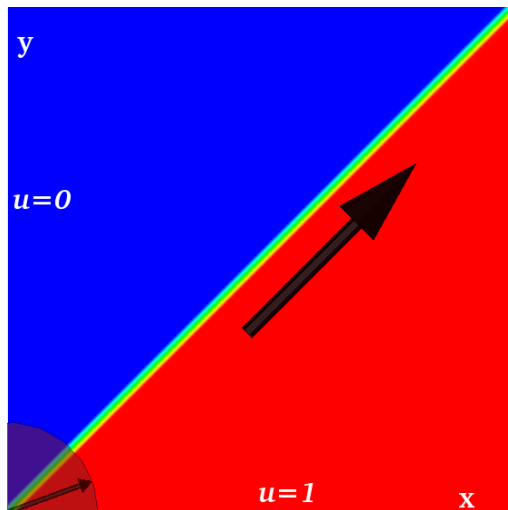


Figure 5: Reference solution for  $\varepsilon = 10^{-5}$  on the domain of interest  $\Omega = [0, 1]^2 \setminus \mathbf{U}_0$  ( $r_0 = 5 \times 10^{-5}$ ).

### Linear solver performance and accuracy

The same numerical experiments as in §7.1 are conducted on this example. The influence of renumbering cells on the linear solver performance for the DG(1) discretization are very similar to the results presented in §7.1 Table 1.

From Figure 6 we can see that the convergence behavior for the approximation of this less regular solution is different from the observations made in §7.1:

1. For the same solution time, the accuracy of DG(1) and SDFEM are comparable.
2. Higher order DG methods are more accurate than SDFEM right from the beginning.
3. With adaptive refinement, higher accuracy is achieved at an earlier stage.

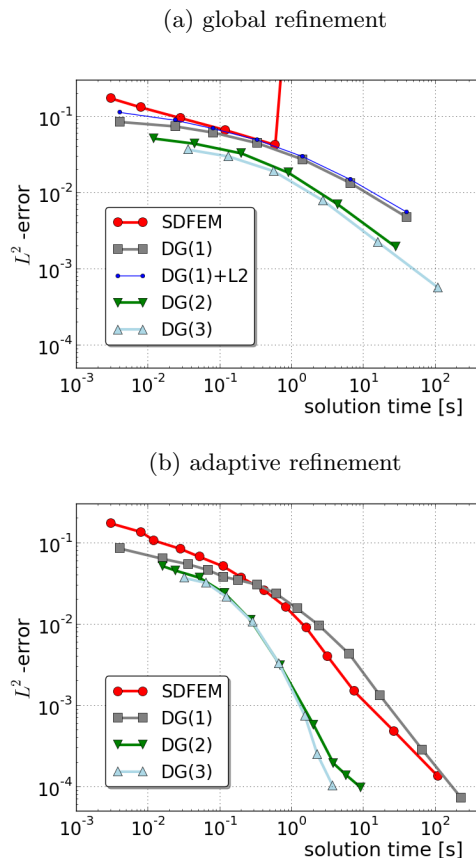


Figure 6: Example by López and Sinusia: (a) global refinement on a structured mesh and (b) adaptive refinement on an unstructured mesh (UG), both starting on a coarse mesh with meshsize  $h_0 = 1/8$ . The refinement fraction for adaptive refinement is  $p_r = 95\%$  (no coarsening). The solution time = matrix assembly time + linear solver time. Linear solver used: BiCGSTAB with SSOR with a reduction of  $10^{-8}$ .

The blue curve (DG(1)+L2) in the first plot is closer to the DG(1) curve than in the example of §7.1 (Figure 4). Furthermore, the SDFEM plot (red curve in Figure 6) stops after 4 refinement steps (16,641 unknowns). In the next refinement step (66,049 unknowns), the iterative lin-

ear solver BiCGSTAB with SSOR converges, but the solution is wrong. In the 6-th step (263, 169 unknowns), the iterative linear solver does not converge, although the linear system can still be solved using the direct solver **SuperLU**. This is most likely due to the fact that the large sparse system has become very ill-conditioned. However, direct solvers are not an option for large practical problems. **SuperLU** has reached the memory limit of the laptop already in the next refinement level where the number of unknowns is 1, 050, 625.

### 7.3 Post-processed DG(1) versus SDFEM

Using the test problem from subsection 7.2, we take a closer look at the quality of the solution with respect to smearing effects and numerical over- and undershoots around the characteristic layer. We compare the post-processed DG(1) method with the SDFEM method on structured meshes. Figure 7 shows the 3-D profile of four different numerical solutions on the whole domain  $[0, 1]^2$ . Figure 8 uses cross-sectional plots over the diagonal line between  $(0, 1)$  and  $(1, 0)$  to zoom into the steep front.

Observations from Figures 7 and 8:

Near the discontinuity in the boundary condition:

1. On the same refinement level, DG(1) exhibits larger over- and undershoots than SDFEM (see Figures 7 (a)+(c)).
2. The diffusive  $L^2$ -projection has a dampening effect on the DG(1) solution, reducing the amount of large over- and undershoots significantly (see Figure 7(c)+(d)) without smearing out the steep front beyond a mesh cell (see Figure 8 solution plots).

Globally:

3. Small over- and undershoots in the DG(1) solution are merely dampened by the diffusive  $L^2$ -Projection (see Figure 8).

4. On the same refinement level, both DG(1) and DG(1)+L2 capture the location of the steep front more accurately than SDFEM throughout the domain (see Figures 7(a)+(c) and 8).
5. SDFEM on refinement level  $L + 1$  captures the steep front as well as DG(1) or DG(1)+L2 on level  $L$  (comparable number of DOF) (see Figure 7(b)+(c) and Figure 8: blue line in (a) vs. red line in (b)).

To achieve a comparable number of DOF as for the DG(1) method, the SDFEM method requires one extra level of global mesh refinement. The resulting matrix assembly time for SDFEM on the refined mesh is higher than for DG(1) on the coarse mesh.

### 7.4 Forward transport in 2-D

In the following, we demonstrate the applicability of the presented DG methods to more realistic scenarios.

We solve the groundwater flow equation (1) for the hydraulic head distribution  $\phi$  and evaluate the velocity field (4) on the structured mesh  $\mathcal{T}_{h_0}$ . The solute transport equation (12) is then solved

- using adaptive DG(1) on a hierarchy of adaptively refined meshes  $\{\mathcal{T}_\nu^{\text{adapt}}\}_{\nu \in \mathbb{N}}$ , or
- using DG( $k$ ) with diffusive  $L^2$ -projection on the same mesh  $\mathcal{T}_{h_0}$ , or
- using SDFEM on the same mesh  $\mathcal{T}_{h_0}$  or on a globally refined mesh  $\mathcal{T}_1^{\text{global}}$ .

The Gaussian field  $Y$  depicted in Figure 9(a) has the physical size of  $100 \times 100[m^2]$ , the resolution of the structured mesh  $\mathcal{T}_0$  is  $100 \times 100$  cells.  $Y$  is described by its mean value  $\beta = -6.0$ , its variance  $\sigma^2 = 1.0$  and the correlation lengths  $(\ell_x, \ell_y) = (10, 10)[m]$ . The hydraulic head is prescribed on the left ( $\phi|_{x=0} = 100[m]$ ) and on the right ( $\phi|_{x=100} = 99.5[m]$ ) boundaries. The induced pressure gradient drives the main flow.

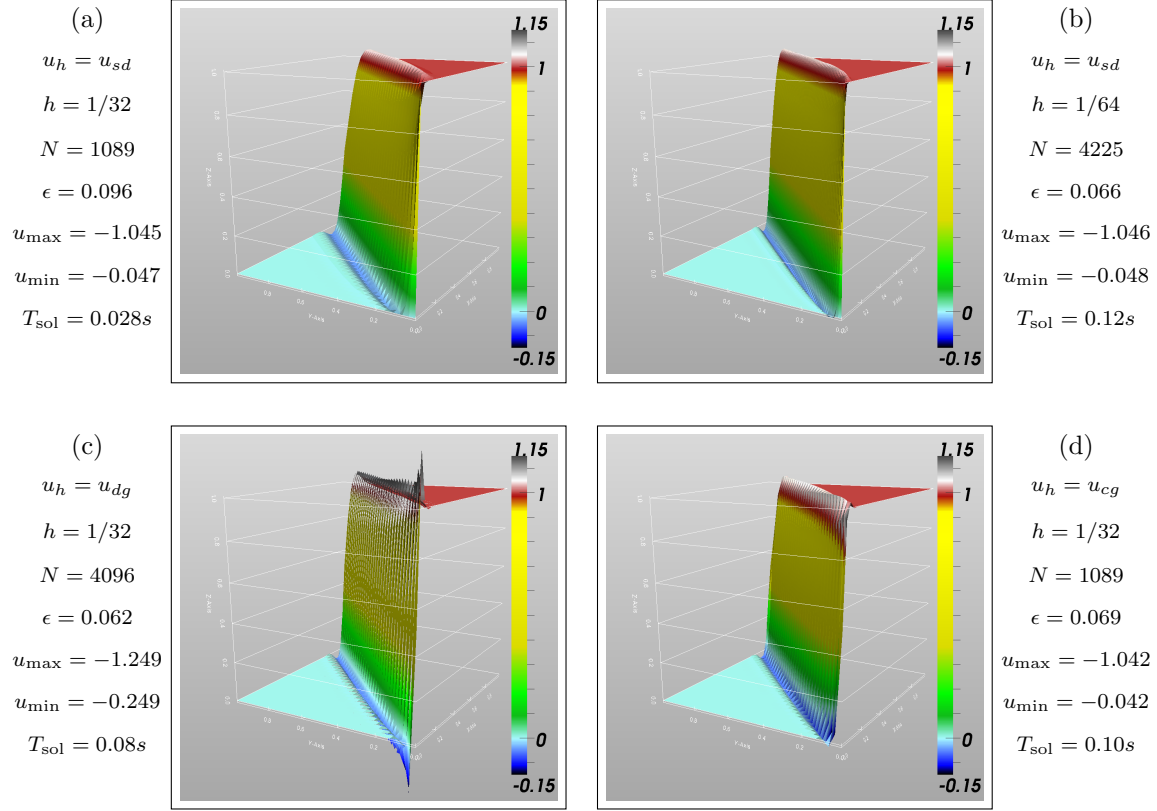


Figure 7: Warped plots (all from the same perspective) of the numerical solution for different methods: (a) and (b):  $u_{sd}$  is the SDFEM solution, (c):  $u_{dg}$  is the DG(1) solution, (d):  $u_{cg}$  is the diffusive  $L^2$ -projection of  $u_{dg}$  (DG(1)+L2).  $h$  is the uniform meshsize,  $N$  is the dimension of the solution space and  $\epsilon = \|u - u_h\|_{L^2(\Omega)}$ .  $u_{\max}$  and  $u_{\min}$  are the maximal and minimal values of the numerical solution  $u_h$ .  $T_{\text{sol}}$  is the solution time (matrix assembly + linear solver).

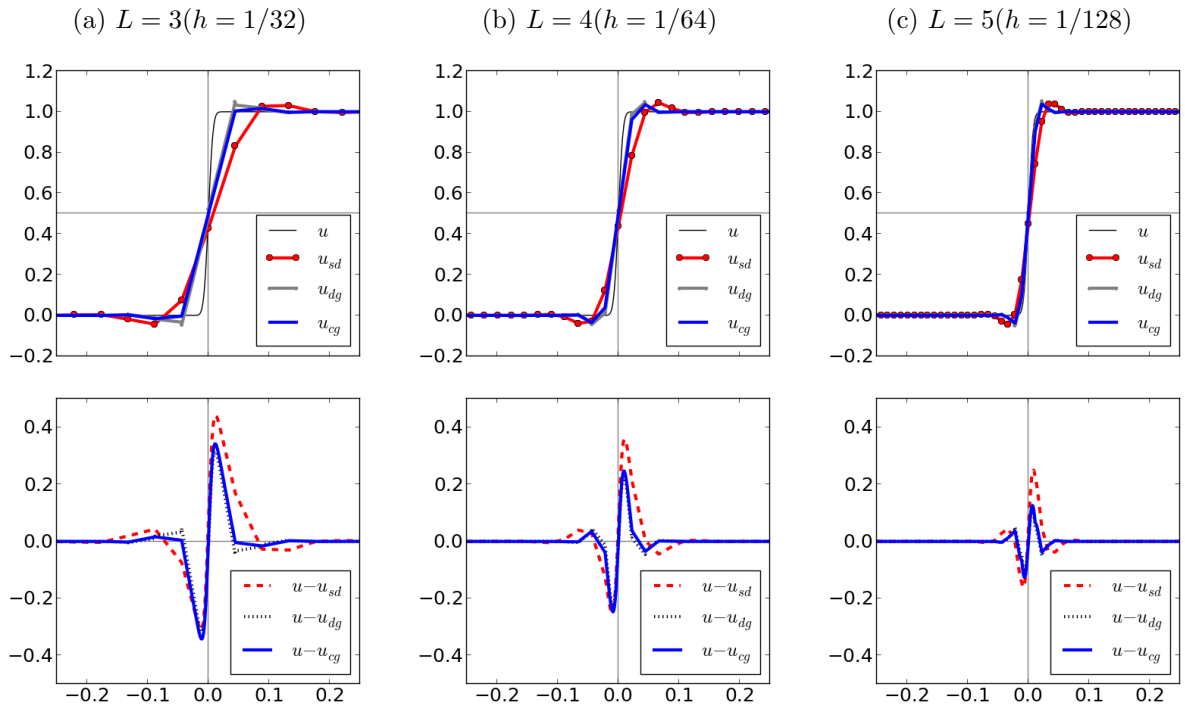


Figure 8: Zoomed plots of the solution and the absolute error for different methods along the diagonal line connecting  $(1,0)$  and  $(0,1)$ .  $L$  is the global refinement level.  $u$  is the true solution resolved on a very fine mesh ( $h = 10^{-5}$ ).

The injection well parameters are  $\tilde{w}_{\text{inj}} = 5 \times 10^{-4}[m^3/s]$ ,  $\tilde{c}_{\text{inj}} = 1[g/m^3]$  and  $T_{\text{inj}} = 100[s]$ . The stationary solution values range between 0 and  $100[gs/m^3]$ . The molecular diffusion is  $D_m = 2 \times 10^{-9}[m^2/s]$ , the longitudinal and transversal dispersivities are  $\alpha_l = 10^{-3}[m]$  and  $\alpha_t = 10^{-4}[m]$ .

Theoretically,  $u_h$  tends to the true solution  $u$  as the meshsize  $h$  tends to 0. At least, all numerical oscillations should disappear if the meshsizes near the characteristic layer become so small that the effective mesh Péclet numbers<sup>4</sup> are smaller than 1. Working with  $\mathcal{O}(\alpha_t) \sim 10^{-4}$  and a base level meshsize  $\mathcal{O}(h) \sim 1$  we would get  $\mathcal{O}(\mathcal{P}_h^t) \sim 10^3$ . It would require 10 levels of global refinement to achieve  $\mathcal{O}(\mathcal{P}_h^t) \sim 1$ , but already after 7 levels of global refinement, our mesh would have more than  $10^8$  cells. The problem size would become extremely large for a 2-D simulation.

Adaptive mesh refinement is the only chance to keep the problem size orders of magnitude lower while reducing mesh Péclet numbers at the step fronts. We choose the stopping criterion (58) from section 4 with a tolerance of  $p_{\text{osc}} = 1\%$ . The result is achieved after 5 steps of adaptive refinement (Table 2 and Figure 9(b)). This solution is taken as the reference solution for assessing the quality of different methods on the structured mesh (Table 3 and Figures 9) and ??).

$L$	DOF	Adaptive DG(1)						
		max. $\mathcal{P}_h^t$	$M[s]$	$T[s]$	$IT$	$TIT$	$u_{\min}$	$u_{\max}$
0	40,000	4675.89	0.91	0.04	4	0.011	134.47	-33.11
1	64,000	2232.44	1.49	0.08	4	0.018	132.26	-31.77
2	102,364	1105.47	2.42	0.25	8	0.033	127.38	-24.68
3	162,964	545.85	3.93	0.75	14	0.050	112.48	-12.10
4	259,372	272.94	6.29	2.29	26	0.076	104.99	-3.39
5	413,860	136.48	10.26	7.29	52	0.110	100.76	-0.38

Table 2: Adaptive mesh refinement on **UG**, with  $p_r = 20[\%]$  and  $p_c = 10[\%]$ . Renumbering mesh cells on mesh level  $L = 5$  takes 0.16 sec. Linear solver used: BiCGSTAB + ILU(0) with reduction  $10^{-8}$ .  $M$  = matrix assembly time,  $IT$  = linear solver iterations,  $T$  = linear solver time

Global $h$ - or $p$ -refinement on a structured mesh						
Method	DOF	$M[s]$	$IT$	$T[s]$	$u_{\min}$	$u_{\max}$
SDFEM ( $L = 0$ )	10,201	0.2	12	0.02	-13.79	116.79
SDFEM ( $L = 1$ )	40,401	0.8	28	0.26	-15.29	113.43
DG(1)	40,000	0.6	4	0.04	-33.11	134.47
diffusive $L^2$ -proj.	10,201	+0.05	1	+0.02	-3.44	103.13
DG(2)	90,000	1.7	4	0.13	-34.04	135.88
diffusive $L^2$ -proj.	10,201	+0.09	1	+0.02	-3.27	104.82
DG(3)	160,000	4.5	4	0.26	-36.69	135.94
diffusive $L^2$ -proj.	10,201	+0.16	1	+0.02	-3.80	103.73

Table 3: Computations on a structured mesh: SDFEM on mesh level  $L = 0$  and  $L = 1$  versus post-processed DG methods on mesh level  $L = 0$  with different polynomial orders. Renumbering mesh cells on  $L = 0$  for the DG methods takes 0.004 sec. Linear solver used for solving the transport equation: BiCGSTAB + ILU(0) with reduction  $10^{-8}$ . Linear solver used for the diffusive  $L^2$ -projection: BiCGSTAB + AMG with reduction  $10^{-8}$ .  $M$  = matrix assembly time,  $IT$  = linear solver iteration number,  $T$  = linear solver time.

<sup>4</sup>Replace  $\alpha_\ell$  by  $\alpha_t$  in (29) to consider longitudinal effects.

2-D solute transport:  $u = m_0^c$

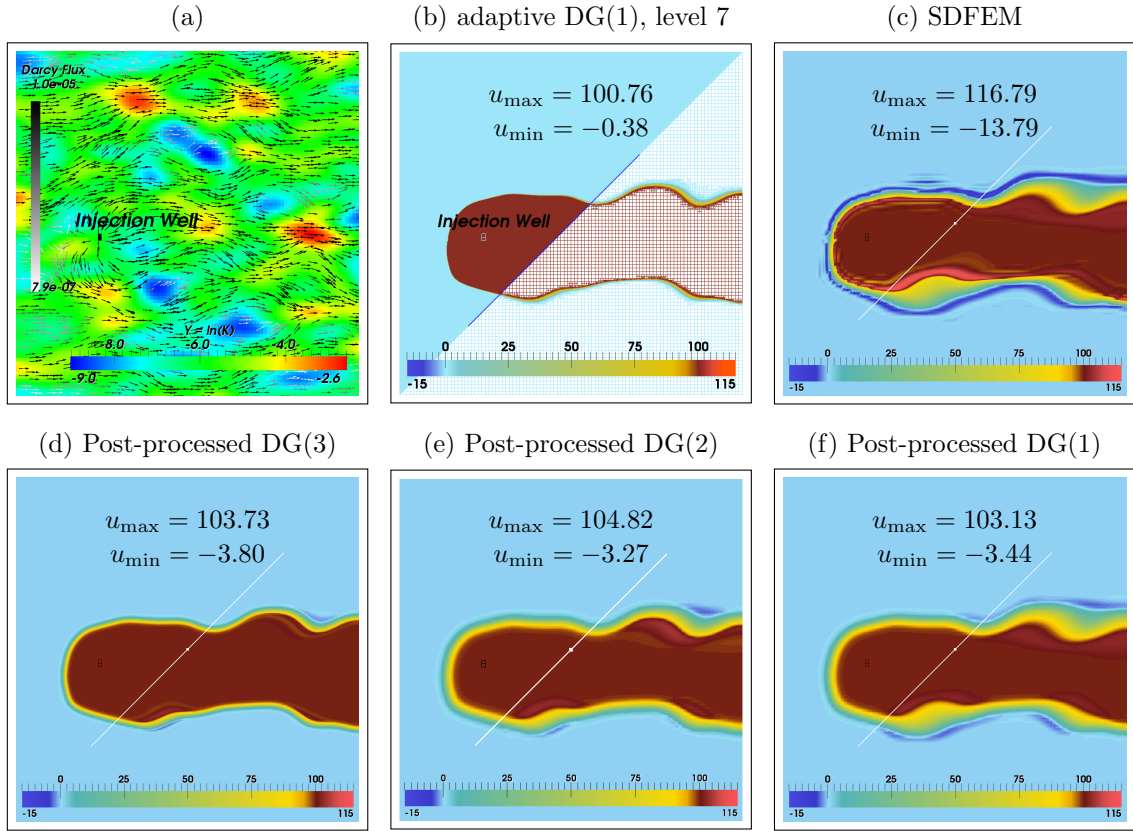


Figure 9: This Figure is continued in Figure 10. (a) Gaussian field  $Y = \ln(K)$  and velocity field  $\vec{q}_h$  on  $\mathcal{T}_0$ . (b) Adaptive DG(1) solution with  $p_{\text{osc}} \leq 1\%$  is taken to be the reference solution for the stationary transport problem. (c) - (f) Comparing different solutions on the coarse structured mesh  $\mathcal{T}_0$  with  $100 \times 100$  cells.

Cross sectional plots along the diagonal line indicated above:

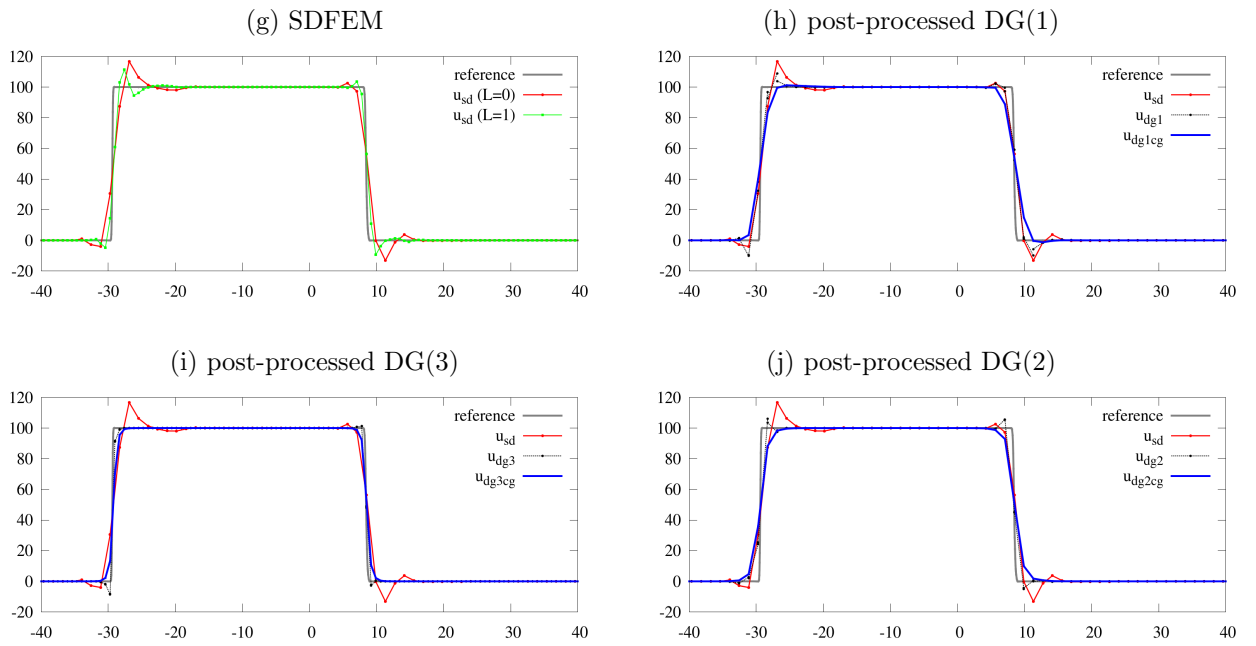


Figure 10: (g) - (j): SDFEM solution  $u_{sd}$  on  $\mathcal{T}_0$  and on  $\mathcal{T}_1^{\text{global}}$  compared to  $DG(k)$  solutions ( $u_{dgk}$ ) on  $\mathcal{T}_0$  and post-processed  $DG(k)$  solutions ( $u_{dgkcg}$ ) on  $\mathcal{T}_0$  along the indicated cut-line (for  $k = 1, 2, 3$ ).  $u_{\max}$  and  $u_{\min}$  are the maximal and minimal values of the numerical solution.

*Observations:*

1. On the coarse mesh  $\mathcal{T}_0$ , DG( $k$ ) solutions with  $k = 1, 2, 3$  may locally exhibit stronger over- and undershoots than the SDFEM solution, but these can be reduced very efficiently with a diffusive  $L^2$ -projection (see the runtimes of  $M$  and  $T$  for the diffusive  $L^2$ -projection in Table 3 and Figure 10(h)-(j)).
2. The over- and undershoots of the SDFEM solution may oscillate into the domain surrounding the steep front (see Figure 9(c)) whereas over- and undershoots of the DG solutions do not show this behavior.
3. On the same mesh  $\mathcal{T}_0$ , higher order polynomials can be used to improve the quality of the DG solution with respect to the sharpness of the steep front. The areas with over- and undershoots are shrunk. A diffusive  $L^2$ -projection preserves this behavior and reduces over- and undershoots (see Figure 9(d)-(f)).
4. The SDFEM method applied to a globally refined mesh  $\mathcal{T}_1^{\text{global}}$  requires a comparable number of unknowns as the DG(1) method on  $\mathcal{T}_0$ . The steep front is resolved similarly well, but the matrix assembly and the linear solution takes longer ( $L = 1$  in Table 3 and Figure 10).

### 7.5 Forward transport in 3-D

A 3-D simulation with a similar setting is started on a coarse mesh  $\mathcal{T}_{h_0}$  with  $32 \times 32 \times 32$  cells. The domain extensions are  $(L_x, L_y, L_z) = (10, 10, 10)[m]$ . The geostatistical field parameters for the Gaussian model are  $\beta = -6.0$ ,  $\sigma^2 = 1.0$  and  $(\ell_x, \ell_y, \ell_z) = (2, 2, 1)[m]$ . The hydraulic head is prescribed on the left boundary by  $\phi|_{x=0} = 10[m]$  and on the right boundary by  $\phi|_{x=10} = 9.8[m]$ . An injection well is placed at the position  $(x, y) = (2.1, 5.1)[m]$  and its  $z$ -range is  $[0 \dots -5][m]$ . The injection well parameters are  $\tilde{w} = 1 \times 10^{-2}[m^3/s]$ ,  $\tilde{c} = 1[g/m^3]$  and

$T_{\text{inj}} = 100[s]$ . The values of the stationary solution range between 0 and  $100[gs/m^3]$ .

Doing the same analysis as for the 2-D case, we find that with global refinement, we would end up with more than  $10^{13}$  cells after 10 refinement steps in order to achieve  $\mathcal{O}(\mathcal{P}_h^t) \sim 1$ . The adaptive DG(1) solution in Table 4 after 9 steps shows a sharp resolution of the steep front (Figure 12(c)). However, there are thin layers where the over- and undershoots exceed 25%. This is still far away from being an acceptable reference solution. To achieve our targeted reduction of under- and overshoots below  $p_{\text{osc}} = 5\%$ , further refinement steps with increasing memory consumption and solution time are necessary.

We make very similar observations as in the 2-D case:

1. The over- and undershoots generated by the DG( $k$ ) solutions with  $k = 1, 2, 3$  can be reduced very efficiently with a diffusive  $L^2$ -projection (see the runtimes of  $M$  and  $T$  for the diffusive  $L^2$ -projection in Table 5).
2. The over- and undershoots of the SDFEM solution may oscillate into the domain surrounding the steep front (see Figure 11(d)) whereas over- and undershoots of the DG solutions do not show this behavior.
3. On the same mesh  $\mathcal{T}_0$ , higher order polynomials can be used to improve the quality of the DG solution with respect to the sharpness of the steep front. The areas with over- and undershoots are shrunk. A diffusive  $L^2$ -projection preserves this behavior and reduces over- and undershoots (see Figure 12(e)+(f)).
4. The SDFEM method applied to a globally refined mesh  $\mathcal{T}_1^{\text{global}}$  requires a comparable number of unknowns as the DG(1) method on  $\mathcal{T}_0$ . The steep front is resolved similarly well (not shown here), but the matrix assembly and the linear solution takes longer ( $L = 1$  in Table 3).

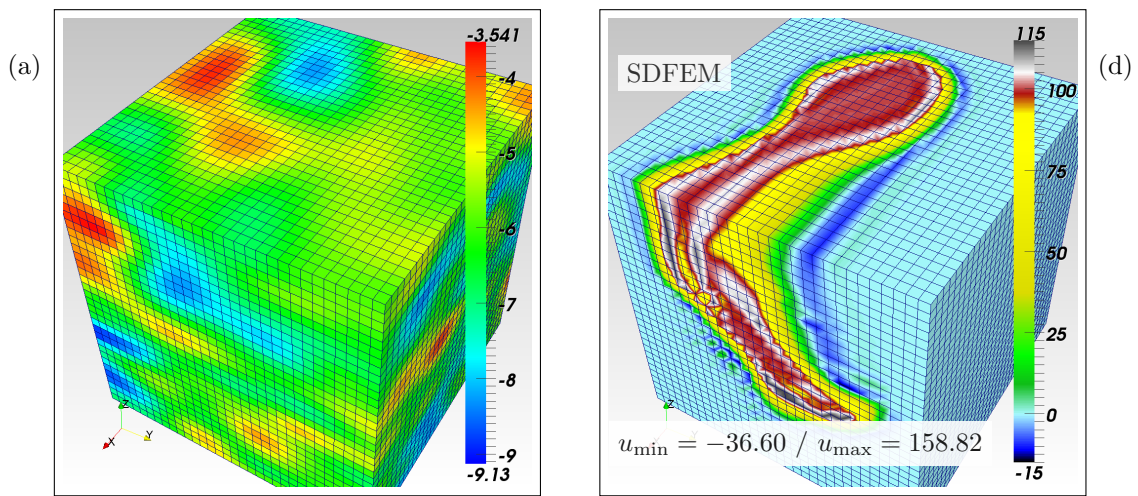


Figure 11: This Figure is continued in Figure 12. (a): Gaussian field  $Y = \ln(K)$  on  $\mathcal{T}_0$  with  $32 \times 32 \times 32$  cells.

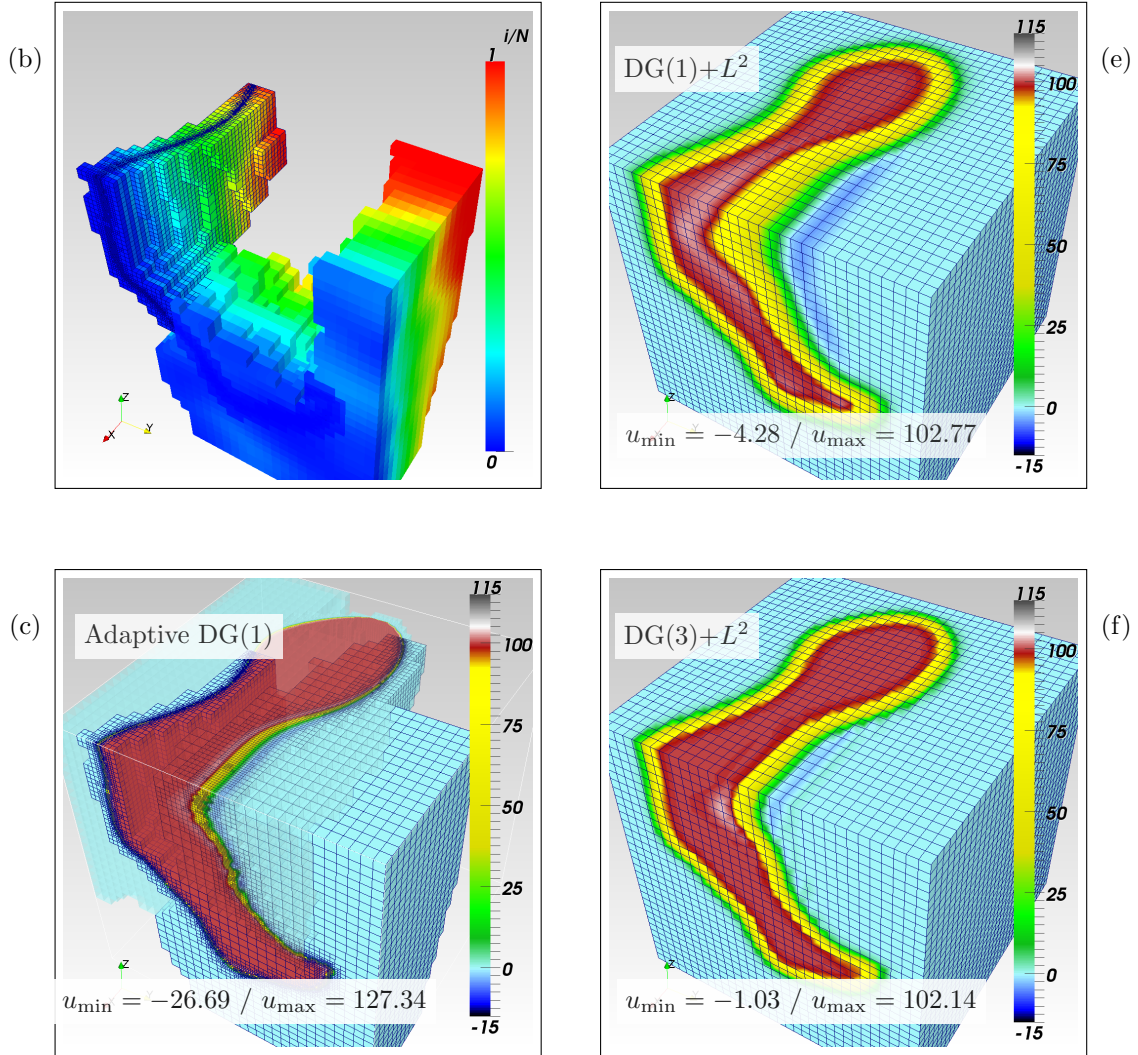


Figure 12: (b)-(c): Illustrating parallel adaptive refinement with dynamic load-balancing (step 9). A reduction of under- and overshoots below 5% is possible, see Table 4. Fig.11(d),Fig.12(e)+(f): Comparing different solutions on the coarse mesh  $\mathcal{T}_0$ .  $u_{\max}$  and  $u_{\min}$  are the maximal and minimal values of the displayed numerical solution.

$L$	Adaptive DG(1)					
	$DOF$	$IT$	$T[s]$	$u_{\min}$	$u_{\max}$	$\mathcal{P}_h^t$
0	346,560	8	0.7	-38.8	136.59	1562
1	399,024	11	1.1	-38.7	142.70	1560
2	537,240	12	1.6	-44.8	144.25	1560
3	814,152	12	3.2	-50.7	141.17	1560
4	1,410,136	18	8.2	-50.2	142.59	389
5	2,740,704	17	15	-56.3	142.78	194
6	5,275,496	18	31	-43.1	147.91	194
7	9,273,552	24	88	-38.8	151.62	97
8	15,368,112	28	152	-28.9	132.08	97
9	23,806,944	35	349	-26.7	127.34	48
10	39,897,040	52	743	-24.0	121.37	48
11	59,903,672	64	1425	-18.7	117.17	24
12	70,498,808	67	1935	-15.2	114.24	24
13	95,837,712	87	3926	-15.5	112.58	24
14	132,771,680	95	5724	-11.7	113.12	24
15	188,298,456	110	8854	-10.5	110.78	24
16	242,272,328	128	13489	-6.88	106.72	24
17	321,793,400	167	28075	-6.59	106.73	24
18	348,929,992	185	30403	-5.30	105.37	24
19	433,481,584	200	38251	-5.23	104.85	12
20	474,804,264	238	61351	-4.98	104.57	12

Table 4: 3-D parallel adaptive refinement on **ALUgrid**, with  $p_r = 70[\%]$  and  $p_c = 5[\%]$ . Renumbering mesh cells on level 20 takes 24.5 sec. Linear solver used: BiCGSTAB + SSOR with reduction  $10^{-8}$ .  $L =$  refinement level,  $IT =$  linear solver iterations,  $T =$  linear solver time. The computation is performed on **quadxeon4**.  $P = 16$  cores are used for the computation, more than 66% of the RAM is required for the linear solver in step 20 alone.

Global $h$ - or $p$ -refinement on a structured mesh						
Method	$DOF$	$M[s]$	$IT$	$T[s]$	$u_{\min}$	$u_{\max}$
SDFEM ( $L = 0$ )	58,806	0.5	14	0.11	-36.6	158.8
SDFEM ( $L = 1$ )	363,350	2.7	22	1.12	-36.5	139.1
DG(1)	376,832	2.3	7	0.38	-37.9	136.4
diffusive $L^2$ -proj.	58,806	+0.2	2	+0.1	-4.3	102.8
DG(2)	1,271,808	22.5	8	3.8	-50.8	146.7
diffusive $L^2$ -proj.	58,806	+0.5	2	+0.1	-3.07	103.4
DG(3)	3,014,656	190.1	9	38.4	-47.1	152.0
diffusive $L^2$ -proj.	58,806	+1.2	2	+0.1	-1.0	102.1

Table 5: 3-D parallel computations with  $P = 8$  cores on **fna** (see Table 6) using a structured mesh with partitioning  $(P_x, P_y, P_z) = (1, 8, 1)$  and overlap = 1. SDFEM on mesh levels  $L = 0$  and  $L = 1$  compared to DG methods on the coarse mesh level  $L = 0$  with different polynomial orders. Parallel renumbering of mesh cells for the DG methods on level  $L = 0$  takes 0.004 sec. Linear solver used for solving the transport equation: BiCGSTAB + ILU(0) with reduction  $10^{-8}$ . Linear solver used for the diffusive  $L^2$ -projection: BiCGSTAB + AMG with reduction  $10^{-8}$ .  $M =$  matrix assembly time,  $IT =$  number of iterations,  $T =$  linear solver time.

## Conclusion and Outlook

For the solution of the steady-state convection-dominant transport equation, we have compared Discontinuous Galerkin (DG) methods to the Streamline Diffusion (SDFEM) method. Putting special emphasis on a practical application, we have analyzed efficiency and accuracy. Two main issues occurring in the solution of the convection-dominated transport equation were tackled:

1. the efficient reduction of numerical under- and overshoots,
2. the efficient solution of the arising linear systems.

With respect to the efficiency (solution time) and the quality of the solution (maximal amplitude of the over- and undershoots and smearing effects at the steep fronts) for the convective-dominant transport problem, the observations made in the sections §7.2–§7.5 favor the combination CCFV / DG(1) + diffusive  $L^2$ -projection over the FEM / SDFEM approach. Considering computing time to be the ultimate measure of available hardware resources, we observed:

- On the same mesh level, the DG solutions resolve the steep fronts more sharply than the SDFEM solution. In order to obtain the same level of accuracy as DG(1), SDFEM would have to work on a globally refined mesh. As a consequence, the SDFEM approach would take longer than DG(1).
- In heterogeneous fields, the layers of spurious oscillations generated by SDFEM may spread into the surrounding domain whereas they stay localized for the DG method.
- The diffusive  $L^2$ -projection is able to reduce the over- and undershoots without increasing smearing effects beyond the mesh size.

Therefore, DG(1) post-processed by a diffusive  $L^2$ -projection offers an efficient and more accurate alternative to the well-known SDFEM method.

Without doubt, the best possible solution in terms of the  $L^2$ -error is achieved with adaptive mesh refinement. However, numerical oscillations can be reduced to an acceptable level only if the mesh cells at the steep front become so small that their local mesh Péclet numbers approach 1 (diffusion-dominant problem). This comes at a very high price, especially in 3-D. A “perfect” solution in this sense may not be necessary for a stable inversion scheme that can cope with noisy data.

Hence, regarding the integration of the forward solvers into an inversion framework, we recommend the combination CCFV / DG(1) post-processed by a diffusive  $L^2$ -projection for the solution of steady-state transport problems with high mesh Péclet numbers. This combination works on the same structured mesh on which the hydraulic conductivity is resolved and keeps the implementation of the inversion scheme simple.

For future developments, a natural extension of the presented methods is a combination of  $h$ - or  $hp$ -adaptive DG with the diffusive  $L^2$ -projection on unstructured meshes (with hanging nodes refinement).

Further improvements regarding efficiency and parallel scalability of the linear solver for the DG discretizations of the transport equation may be achieved by a multilevel preconditioner in which the block Gauss-Seidel method with downwind numbering plays the role of a smoother [Kanschat, 2008b].

We have seen in Tables 3 and 5 that the number of unknowns and therefore the matrix assembly and linear solver times for DG( $k$ ) grow rapidly with the order  $k$  of the polynomial basis. On quadrilateral/hexahedral meshes, where quadrature points and shape functions can be constructed from a tensor product of 1-D objects, an excellent boost in performance can be achieved for the matrix assembly part with a technique called sum-factorization [Melenk et al., 2001].

## Appendix

Machine name	quadxeon4	fna
Number of nodes	1	1
RAM per node	1024 GB (DDR-3/1066)	128GB (DDR-3/1333 MHz)
CPU-sockets per node	4	4
Total #cores	40	48
OS	Debian GNU 7	Debian GNU 7
CPU socket	Intel® Xeon® E7-4870	AMD Opteron™ 6172
Clock speed	2.40 GHz	2.10 GHz
#cores	10	12
#threads	20	12
Launch date	Q2/2011	Q1/2010
L3 Cache	30 MB	12 MB
#memory channels	4	4

Table 6: Single-node multi-core machines at the IWR Heidelberg

## Acknowledgements

This study has been funded by the Baden-Württemberg Stiftung in its high-performance computing program, contract HPC-8.

## References

- Augustin, M., Caiazzo, A., Fiebach, A., Fuhrmann, J., John, V., Linke, A., Umla, R., 2011. An assessment of discretizations for convection-dominated convection-diffusion equations. *Computer Methods in Applied Mechanics and Engineering* 200, 3395–3409.  
URL <http://dx.doi.org/10.1016/j.cma.2011.08.012>
- Bastian, P., 2011. Benchmark 3D: Symmetric Weighted Interior Penalty Discontinuous Galerkin Scheme. In: Först, J., Fürst, J., Halama, J., Herbin, R., Hubert, F. (Eds.), *Finite Volumes for Complex Applications VI Problems & Perspectives*. Vol. 4 of Springer Proceedings in Math. Springer Berlin Heidelberg, pp. 949–959.  
URL [http://dx.doi.org/10.1007/978-3-642-20671-9\\_92](http://dx.doi.org/10.1007/978-3-642-20671-9_92)
- Bastian, P., Birken, K., Lang, S., Johannsen, K., Neuß, N., Rentz-Reichert, H., Wieners, C., 1997. UG: A flexible software toolbox for solving partial differential equations. *Computing and Visualization in Science* 1, 27–40.  
URL <http://www.iwr.uni-heidelberg.de/iwrwikiequipment/software/ug>
- Bastian, P., Blatt, M., Dedner, A., Engwer, C., Fahlke, J., Gräser, C., Klöforn, R., Nolte, M., Ohlberger, M., Sander, O., 2011. DUNE Web page. <http://www.dune-project.org>.
- Bastian, P., Blatt, M., Dedner, A., Engwer, C., Klöforn, R., Kornhuber, R., Ohlberger, M., Sander, O., 2008a. A Generic Grid Interface for Parallel and Adaptive Scientific Computing. Part II: Implementation and Tests in DUNE. *Computing* 82 (2–3), 121–138.  
URL <http://www.springerlink.com/content/gn177r643q2168g7/>
- Bastian, P., Blatt, M., Dedner, A., Engwer, C., Klöforn, R., Ohlberger, M., Sander, O., 2008b. A Generic Grid Interface for Parallel and Adaptive Scientific Computing. Part I: Abstract Framework. *Computing* 82 (2–3), 103–119.  
URL <http://www.springerlink.com/content/4v77662363u41534/>
- Bear, J., Cheng, A.-D., 2010. *Modeling Groundwater Flow and Contaminant Transport*. Vol. 23 of *Theory and Applications of Transport in Porous Media*. Springer.
- Bey, J., Wittum, G., 1997. Downwind numbering: robust multigrid for convection-diffusion problems. *Applied Numerical Mathematics* 23, 177–192.  
URL [http://dx.doi.org/10.1007/978-3-663-14125-9\\_5](http://dx.doi.org/10.1007/978-3-663-14125-9_5)
- Blatt, M., 2010. *A Parallel Algebraic Multigrid Method for Elliptic Problems with Highly Discontinuous Coefficients*. PhD Thesis, Heidelberg University.  
URL <http://nbn-resolving.de/urn:nbn:de:bsz:16-opus-108562>
- Brezzi, F., Fortin, M., 1991. *Mixed and Hybrid Finite Elements*. Springer-Verlag, New York.

- Brooks, A. N., Hughes, T. J. R., 1982. Streamline upwind/Petrov-Galerkin formulations for convection dominated flows with particular emphasis on the incompressible Navier-Stokes equations. *Computer Methods in Applied Mechanics and Engineering* 32(1-3), 199–259.  
URL [http://dx.doi.org/10.1016/0045-7825\(82\)90071-8](http://dx.doi.org/10.1016/0045-7825(82)90071-8)
- Cirpka, O. A., Kitanidis, P. K., 2001. Sensitivity of temporal moments calculated by the adjoint-state method and joint inverting of head and tracer data. *Advances in Water Resources* 24, 89–103.  
URL [http://dx.doi.org/10.1016/S0309-1708\(00\)00007-5](http://dx.doi.org/10.1016/S0309-1708(00)00007-5)
- Couto, P., Malta, S., 2008. Interaction between sorption and biodegradation processes in the contaminant transport. *Ecological Modelling* 214(1), 65–73.  
URL <http://dx.doi.org/10.1016/j.ecolmodel.2008.01.012>
- De Marsily, G., 1986. *Quantitative Hydrogeology: Groundwater Hydrology for Engineers*. Academic Press.
- Dedner, A., Klöforn, R., Nolte, M., 2014. The dune-alugrid module. CoRR abs/1407.6954.  
URL <http://arxiv.org/abs/1407.6954>
- Elman, H. C., Silvester, D. J., Wathen, A. J., 2005. *Finite Elements and Fast Iterative Solvers with Applications in Incompressible Fluid Dynamics*. Oxford University Press.
- Ern, A., Stephansen, A., Vohralík, M., 2010. Guaranteed and robust discontinuous galerkin a posteriori error estimates for convection-diffusion-reaction problems. *Journal of Comp. and Appl. Math.* 234(1), 114–130.  
URL <http://dx.doi.org/10.1016/j.cam.2009.12.009>
- Ern, A., Stephansen, A. F., Zunino, P., 2008. A discontinuous Galerkin method with weighted averages for advection-diffusion equations with locally small and anisotropic diffusivity. *IMA Journal of Numerical Analysis* 29, 235–246.  
URL <http://dx.doi.org/10.1093/imanum/drm050>
- Georgoulis, E. H., Hall, E., Houston, P., 2009. Discontinuous Galerkin Methods on hp-Anisotropic Meshes II: A Posteriori Error Analysis and Adaptivity. *Applied Numerical Mathematics* 59(9), 2179 – 2194.  
URL <http://dx.doi.org/10.1016/j.apnum.2008.12.008>
- Gordon, E., Shamir, U., Bensabat, J., 2000. Optimal management of a regional aquifer under salinization conditions. *Water Resources Research* 36, 3193–3203.  
URL <http://dx.doi.org/10.1029/2000WR900177>
- Hackbusch, W., Probst, T., 1997. Downwind Gauß-Seidel smoothing for convection dominated problems. *Numerical Linear Algebra with Applications* 4(2), 85–102.  
URL [http://dx.doi.org/10.1002/\(SICI\)1099-1506\(199703/04\)4:2<85::AID-NLA100>3.0.CO;2-2](http://dx.doi.org/10.1002/(SICI)1099-1506(199703/04)4:2<85::AID-NLA100>3.0.CO;2-2)
- Harvey, C., Gorelick, S., 1995. Temporal moment-generating equations: modeling transport and mass-transfer in heterogeneous aquifers. *Water Res. Research* 31(8), 1895–1911.  
URL <http://dx.doi.org/10.1029/95WR01231>
- Hughes, T. J., Mallet, M., Akira, M., 1986. A new finite element formulation for computational fluid dynamics: II. Beyond SUPG. *Computer Methods in Applied Mechanics and Engineering* 54(3), 341–355.  
URL [http://dx.doi.org/10.1016/0045-7825\(86\)90110-6](http://dx.doi.org/10.1016/0045-7825(86)90110-6)
- John, V., 2000. A numerical study of a posteriori error estimators for convection-diffusion equations. *Comp. Methods in Appl. Mechanics and Engineering* 190, 757–781.  
URL [http://dx.doi.org/10.1016/S0045-7825\(99\)00440-5](http://dx.doi.org/10.1016/S0045-7825(99)00440-5)
- John, V., Knobloch, P., 2007a. On spurious oscillations at layers diminishing (SOLD) methods for convection-diffusion equations: Part I. *Computer Methods in Applied Mechanics and Engineering* 196, 2197–2215.  
URL <http://dx.doi.org/10.1016/j.cma.2006.11.013>

- John, V., Knobloch, P., 2007b. On the performance of SOLD methods for convection-diffusion problems with interior layers. *Internat. Journal of Comp. Science and Math.* 1(2-4), 245–258.  
URL <http://dx.doi.org/10.1504/IJCSM.2007.016534>
- John, V., Knobloch, P., 2008. On spurious oscillations at layers diminishing (SOLD) methods for convection-diffusion equations: Part II - Analysis for P1 and Q1 finite elements. *Comp. Methods in Appl. Mechanics and Engineering* 197(21-24), 1997–2014.  
URL <http://dx.doi.org/10.1016/j.cma.2007.12.019>
- John, V., Maubach, J., Tobiska, L., 1997. Non-conforming streamline-diffusion-finite-element-methods for convection-diffusion problems. *Numerische Mathematik* 78(2), 165–188.  
URL <http://dx.doi.org/10.1007/s002110050309>
- John, V., Schmeyer, E., 2008. Finite element methods for time-dependent convection-diffusion-reaction equations with small diffusion. *Computer Methods in Applied Mechanics and Engineering* 198, 475–494.  
URL <http://dx.doi.org/10.1016/j.cma.2008.08.016>
- John, V., Schmeyer, E., 2009. On Finite Element Methods for 3D Time-Dependent Convection-Diffusion-Reaction Equations with Small Diffusion. *BAIL 2008 - Boundary and Interior Layers: Lecture Notes in Computational Science and Engineering* 69, 173–181.  
URL [http://dx.doi.org/10.1007/978-3-642-00605-0\\_13](http://dx.doi.org/10.1007/978-3-642-00605-0_13)
- Kanschat, G., 2008a. *Discontinuous Galerkin Methods for Viscous Incompressible Flow*. *Advances in Numerical Mathematics*. Springer.
- Kanschat, G., 2008b. Robust smoothers for high-order discontinuous Galerkin discretizations of advection-diffusion problems. *Journal of Comp. and Appl. Math.* 218(1), 53–60.  
URL <http://dx.doi.org/10.1016/j.cam.2007.04.032>
- Kuzmin, D., 2006. On the design of general-purpose flux limiters for implicit FEM with a consistent mass matrix. I. Scalar convection. *Journal of Computational Physics* 219(2), 513–531.  
URL <http://dx.doi.org/10.1016/j.jcp.2006.03.034>
- Kuzmin, D., 2009. Explicit and implicit FEM-FCT algorithms with flux linearization. *Journal of Computational Physics* 228(7), 2517–2534.  
URL <http://dx.doi.org/10.1016/j.jcp.2008.12.011>
- Kuzmin, D., 2010. *A Guide to Numerical Methods for Transport Equations*. Accessed: 2014-08-29.  
URL <http://www.mathematik.uni-dortmund.de/~kuzmin/cfdbook.html>
- López, J. L., Sinusía, E. P., 2004. Asymptotic expansions for two singularly perturbed convection-diffusion problems with discontinuous data: The quarter plane and the infinite strip. *Studies in Applied Mathematics* 113, 57 – 89.  
URL <http://dx.doi.org/10.1111/j.1467-9590.2004.01508.x>
- Melenk, J., Gerdes, K., Schwab, C., 2001. Fully discrete hp-finite elements: fast quadrature. *Comput. Meth. in Appl. Mech. & Engineering* 190 (32-33), 4339–4364.  
URL [http://dx.doi.org/10.1016/S0045-7825\(00\)00322-4](http://dx.doi.org/10.1016/S0045-7825(00)00322-4)
- Nowak, W., Cirpka, O. A., 2006. Geostatistical inference of hydraulic conductivity and dispersivities from hydraulic heads and tracer data. *Water Res. Research* 42 (8).  
URL <http://dx.doi.org/10.1029/2005WR004832>
- Pietro, D. A. D., Ern, A., 2012. *Mathematical Aspects of Discontinuous Galerkin Methods*. Springer.
- Raviart, P. A., Thomas, J. M., 1977. *Mathematical aspects of finite element methods*. *Lecture Notes in Mathematics* 606, 292 – 315.  
URL <http://dx.doi.org/10.1007/BFb0064470>
- Reed, W., Hill, T., 1973. *Triangular mesh methods for the neutron transport equation*. Technical Report LA-UR-73-479, Los Alamos Scientific Laboratory.

- Rivière, B., 2008. Discont. Galerkin Methods for Solving Elliptic and Parabolic Equations: Theory and Implementation. SIAM.
- Roos, H., Stynes, M., Tobiska, L., 2008. Robust Numerical Methods for Singularly Perturbed Differential Equations. Springer.
- Roth, K., 2012. Soil Physics. Lecture Notes: Institute of Environmental Physics, Heidelberg University.  
 URL <http://www.iup.uni-heidelberg.de/institut/forschung/groups/ts/students/sp>
- Scheidegger, A. E., 1961. General theory of dispersion in porous media. Journal of Geophysical Research 66 (10), 3273 – 3278.  
 URL <http://dx.doi.org/10.1029/JZ066i010p03273>
- Schötzau, D., Zhu, L., 2009. A robust a-posteriori error estimator for discontinuous Galerkin methods for convection-diffusion equations. Applied Num. Math. 59(9), 2236–2255.  
 URL <http://dx.doi.org/10.1016/j.apnum.2008.12.014>
- Verfürth, R., 1998. A posteriori error estimators for convection-diffusion equations. Numerische Mathematik, Springer 80, 641–663.  
 URL <http://dx.doi.org/10.1007/s002110050381>
- Verfürth, R., 2005. Robust a posteriori error estimates for stationary convection-diffusion equations. SIAM Journal on Numerical Analysis 43(4), 1766–1782.  
 URL <http://dx.doi.org/10.1137/040604261>
- Zhu, L., Schötzau, D., 2011. A robust a-posteriori error estimate for hp-adaptive DG methods for convection-diffusion equations. IMA Journ. of Num. Analysis 31(3), 971 – 1005.  
 URL <http://dx.doi.org/10.1093/imanum/drp038>